ALMA MATER STUDIORUM
UNIVERSITÀ DI BOLOGNA

Department of Industrial Engineering

Second Cycle Degree in
AEROSPACE ENGINEERING

Reconstruction of Rosetta's relative orbit around comet Churyumov-Gerasimenko using radiometric measurements

Dissertation in ING-IND /05: Spacecraft Orbital Dynamics and Control

Supervisor
Prof. Riccardo Lasagni Manghi

Defended by
Federico Scalera

Co-Supervisors
Prof. Marco Zannoni
Prof. Luis Antonio Gomez Casajus

19 / March / 2025

Academic Year 2024/2025

Abstract

The Rosetta mission escorted the comet 67P Churyumov-Gerasimenko while it passed close to the Sun, to study the behaviour of these fascinating objects. The dynamical environment of 67P is complex and dictated by the comet itself. Indeed, the most potent force felt by the probe is the gravity of the small body, which is highly irregular. Another phenomenon the S/C has to go through is the coma drag, i.e. the acceleration induced on the probe by the interaction between its surface and the atmosphere generated by the comet's outgassing, which becomes more active as it gets closer to the Sun.

Radiometric measurements of the mission have been used to configure a preliminary model aimed at performing radioscience analyses with the data collected by the Rosetta mission. After processing the mission's raw measurements, an observational model was created and tested using a passthrough process. Such procedure allowed us to understand the major sources of errors in the generation of computed observables, namely the steerable high gain antenna, the on-board transponder bias and the ground station biases. Consequently, the dynamical model has been built modelling the gravity sources involved, the solar radiation pressure and the manoeuvres. The contribution of the coma drag has been accounted for by using stochastic accelerations, defined as 2-hour batches in which they assume constant value. Finally, the setup has been tested by performing estimations on Rosetta's state, its orbital and desaturation manoeuvres and the location of the phase centre of its high gain antenna. The results obtained by these estimations have been compared with the ones provided by Rosetta's navigation team. A mission arc going from the 22^{nd} to the 28^{th} of September 2014 was selected, in which Rosetta is already bound to the comet, but at the same time, it does not get too close to the celestial body. The estimations proved the reliability of the implemented models while highlighting the limits of using only the radiometric measurements.

Contents

List of Figures

List of Tables

Acronyms

APM	Antenna Pointing Mechanism
AU	Astronomical Unit
BOA	Binary Object Archive
DOR	Differential One-way Ranging
DSN	Deep Space Network
EME2000	Earth Mean Equator at J2000
ESA	European Space Agency
G/S	Ground Station
HGA	High Gain Antenna
IFMS	Intermediate Frequency Modulation System
LGA	Low Gain Antenna
MGA	Medium Gain Antenna
MONTE	Mission-analysis and Operations Navigation Toolkit Environment
NASA	National Aeronautics and Space Administration
OD	Orbit Determination
OM	Orbital Maneuver
OPNAV	Optical Navigation
PDF	Probability Density Function
PLL	Phase-Locked Loop
RMS	Root Mean Square
S/C	Spacecraft
SA	Solar Array
SRP	Solar Radiation Pressure

SSB	Solar System Barycenter
PLL	Phase Locked Loop
TDM	Tracking Data Message
UNIBO	University of Bologna
USO	Ultra Stable Oscillator

Chapter 1

Introduction

1.1 The Rosetta mission

1.1.1 Overview

The Rosetta mission is a deep space mission developed by the European Space Agency (ESA) in collaboration with several European national space agencies and the National Aeronautics and Space Administration (NASA). Rosetta is part of ESA's long-term programme Horizon 2000 [1] and was launched by an Ariane 5 from the Guyana Space Center in Kourou, French Guyana, on March 2, 2004. Its general objective was to investigate the origin of our solar system thanks to an intensive analysis campaign of the comet 67P Churyumov-Gerasimenko.

To reach the comet, the spacecraft made a long deep space journey where three Earth swing-bys [8], one Mars swing-by [9] and two asteroid flybys [10, 11] had been performed and then it entered a long hibernation period that ended with its reactivation on January 20, 2014, nearly 10 years after launch.

Once awake, Rosetta targeted the comet and approached it on August 6, 2014 [12]. The spacecraft also hosted a lander called Philae, which was successfully delivered on the surface of 67P after few months of observations and experiments [13]. Afterwards, Rosetta continued its scientific mission while the comet passed through its perihelion and moved towards the outer Solar system once again, allowing us to study its activity evolution [14].

Finally, the mission came to an end due to the great distance from both Earth and Sun. On 30 September, 2016, Rosetta landed on the comet interrupting its communications [15].

1.1.2 Scientific objectives

Initially planned as a sample and return mission, the main goal of the Rosetta mission was to investigate the origin of our solar system by studying the origin of comets. Due to time and budget constraints, the mission sample and return hypothesis were discarded and the main goals of the mission were to orbit around the comet during its close passage to the Sun to deeply study and better understand the activities that these objects go through. In the meantime, Philae, the lander, was meant to study the composition of the comet's nucleus by lying on its surface.

The comet chosen as mission's target is *67P Churyumov-Gerasimenko*, a comet approximately 4 km large, being part of the Jupiter family, i.e. the ensemble of comets with a period lower than 20 years and small inclination with respect to the ecliptic. Indeed 67P's orbital period and inclination are 6.43 years and 3.8 degrees respectively. 67P was first observed in 1969 by two astronomers, Klim Ivanovych Churyumov and Svetlana Ivanovna Gerasimenko, using photographic plates. Its shape consists of two lobes connected by a thinner neck. There is the possibility that it formed from a collision between two separate bodies that fused and for this reason it is called *contact binary*. A picture of Churyumov-Gerasimenko is shown in Figure 1.1.

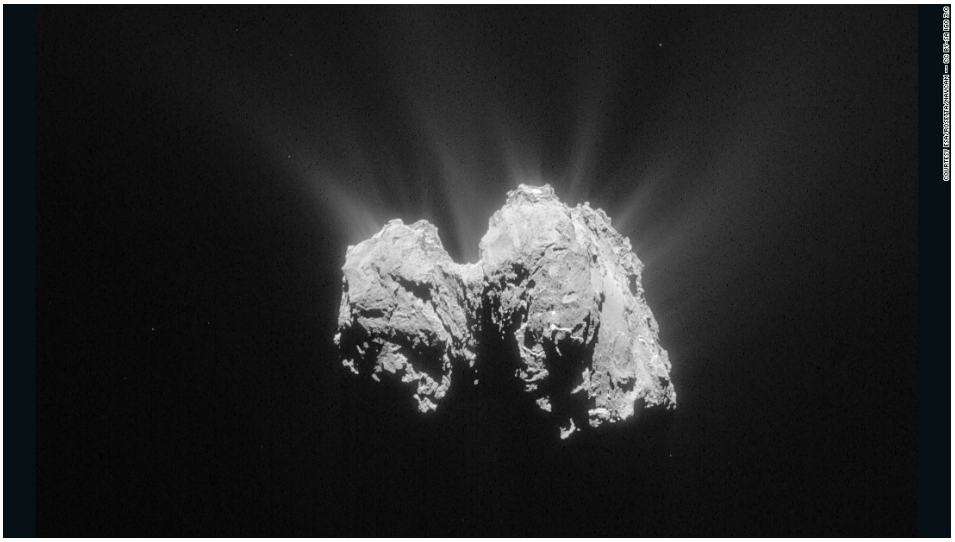

Figure 1.1: A view of comet 67P Churyumov-Gerasimenko from Rosetta Navigation Camera

1.1.3 Rosetta spacecraft and body frame

The Rosetta Spacecraft [1] is built around a central cuboid frame measuring 2.8 m × 2.1 m × 2.0 m, with an aluminium honeycomb platform. Its launch mass is 2900 kg, which includes the 100 kg lander (Philae) and 165 kg of scientific instruments. Two 32 m^2 solar panels extend from opposite sides, spanning a total of 32 m tip-to-tip.

The spacecraft has two main modules: one for the scientific instruments (payload support module) and one for the spacecraft systems (bus support module). A steerable High-Gain Antenna (HGA) of 2.2 m in diameter is mounted on one side, while the lander is attached to the opposite side. The science instruments are positioned to continuously face the comet, while the solar panels and antennae face the Sun and Earth respectively. Radiators and louvres are installed on the parts that do not face the Sun or comet.

A vertical thrust tube at the bottom of the spacecraft holds two tanks containing a total of 1720 kg of propellant and oxidizer. This fuel is used to provide a speed increment of 2200 m/sec during the mission. Rosetta is three-axis stabilized using 24 thrusters, reaction wheels, star trackers, sun sensors, navigation cameras, and

laser gyros. The solar arrays generate 395 W at 5.25 AU and 850 W at 3.4 AU, with energy stored in four 10 Ah batteries. Other than the HGA, communication is maintained through a Medium-Gain Antenna (MGA), and two Low-Gain Antennas (LGA) using S- and X-band links.

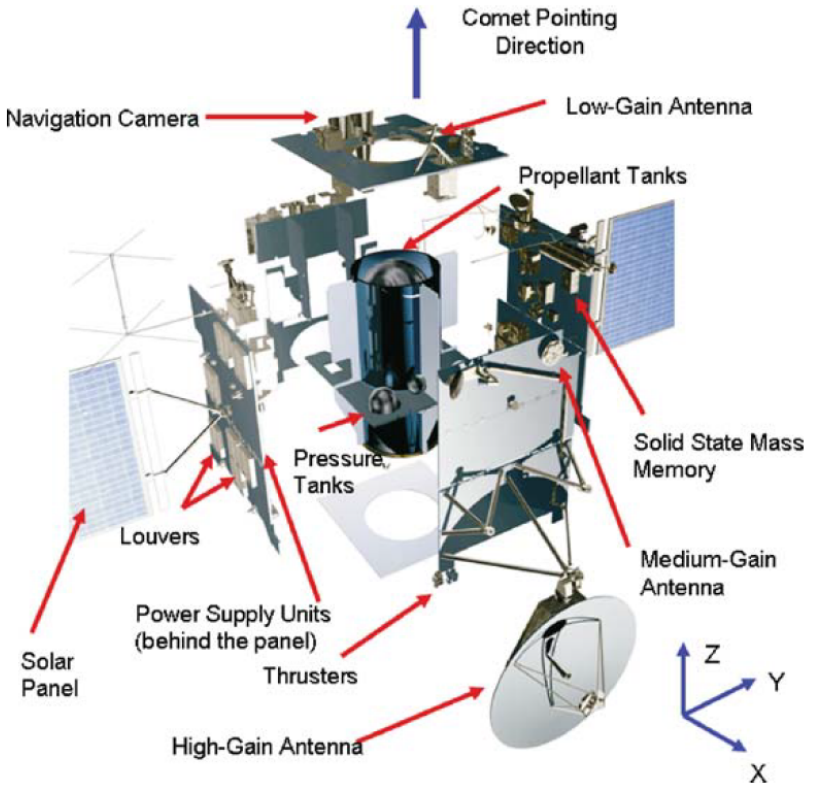

Figure 1.2: The Rosetta Spacecraft, an exploded view [1]

The payload of the Rosetta orbiter is composed of the following instruments:

- *ALICE*, an ultraviolet imaging spectrometer used to analyse gases in the coma and tail of the comet, providing also information on the surface composition of the comet's nucleus
- *CONSERT*, a sounding experiment using radiowaves to study the interior of the comet
- *COSIMA*, an ion mass analyser to study the features, like the composition, of dust grains emitted by the comet
- *GIADA*, the grain impact analyser and dust accumulator, used to measure number, mass, momentum and velocity distribution of dust grains
- *MIDAS*, a micro-imaging dust analysis system that studied the particle's population, size, volume and shape
- *MIRO*, the microwave instrument to study comet's gasses and sub-surface

- *OSIRIS*, an optical, spectroscopic, and infrared remote imaging system aimed at taking high-resolution images of the nucleus
- *ROSINA*, the orbiter spectrometer for ion and neutral species analysis used to study the comet's atmosphere and ionosphere
- *RPC* was a complex of five instruments whose objective is to study the interaction of the comet and solar wind and the physical properties of the nucleus
- *VIRTIS*, a visible and infrared mapping spectrometer that mapped and studied the nature of the solids and temperature on the surface
- *SREM*, a standard radiation environment monitor that analyzed the high energetic particles encountered by Rosetta
- *RSI*, i.e. the Radioscience investigation using the telecommunication equipment onboard

Regarding radioscience, the mission focused on using radiometric measurements, especially Doppler, to investigate the nucleus and inner coma drag of the comet [16]. One of the main goals of these experiments was to model the 67P's gravity field and mass distribution in terms of mass, bulk density, gravity coefficient, moments of inertia and spin rate. About its motion, the RSI experiments needed to characterize the heliocentric orbit and lightshift. In addition, also the thermal properties of the comet were to be studied. Also, the cometary nucleus was deeply observed using the telecommunication subsystem. The main goals were to model its size and shape, internal structure, dielectric constant, surface roughness and rotational motion. Finally, the cometary coma was also an object of interest for the RSI experiments, since using the spacecraft's antennas allowed us to characterize its plasma content and the flux of gas and mass. All these observations were aided by the optical navigation system.

For the purposes of this work, it is convenient to state how the body frame of Rosetta is defined [17]:

- +Z axis is perpendicular to the launch vehicle interface plane and points toward the payload side
- +X axis is perpendicular to the HGA mounting plane and points toward the HGA
- +Y axis completes the right-handed frame and is parallel to the solar panels rotation axis
- the origin of this frame is the launch vehicle interface point

1.1.4 Pre-lander-delivery phase

This thesis is focused on the period that goes from Rosetta's arrival at the comet in August 2014 to the last days before Philae's delivery at the end of October

2014. During this phase, the main goal of the mission was to make observations of 67P's surface to improve optical navigation. In particular, surface observations were intended to generate a sufficient number of *landmarks*: recognisable surface features that the optical navigation system can use to determine the state of the spacecraft concerning the comet [3].

During these months, the mission went through five phases:

- *Close approach trajectory*: the probe moves on hyperbolic arcs in front of the illuminated side of the comet at 100 km distance initially and at 60 km afterwards; the first landmarks are generated during this phase
- *Transition to global mapping phase*: transfer trajectory to the following phase
- *Global mapping phase*: Rosetta is placed on 30 Km orbits with a large solar phase angle (angle between comet to probe vector and comet to Sun vector) where it maps the visible side of the comet
- *Close observation phase*: aiming to improve the knowledge of the comet's centre of mass and gravity field, the probe flies on closer orbits with 90 degrees solar phase angle (i.e. in the so-called *terminator plane*) at 20 Km first and 10 Km then.
- *Science surface package delivery phase*: the spacecraft moves away on a 30 Km orbit from which the lander delivery manoeuvre will start.

1.2 The orbit determination process

Orbit determination is a crucial part of the navigation process, aimed at reconstructing a probe's past trajectory and predicting the future one using measurements provided up to the so-called data cut-off. This is done by estimating *solve-for parameters*, such as spacecraft state, celestial bodies' states, manoeuvres and gravity field parameters. Thus, the parameters uniquely defining the trajectory using a dynamical model.

Raw measurements, or *observed observables*, provide the data for this process. In particular, they are compared against *computed observables* generated using mathematical models. The differences between observed and computed observables are called *residuals*. An estimation filter minimizes them by iteratively refining the model until acceptable residuals are achieved. Iterative adjustments are necessary due to real-world non-linearity, ensuring accurate trajectory reconstruction and prediction. The final solution of an orbit determination process is the set of *solve-for* parameters that minimizes the residuals, together with a *covariance matrix* containing the uncertainties of the solution itself.

Orbit determination uses three types of solve-for parameters:

- *Dynamical parameters*, changing over time via deterministic models (e.g., spacecraft state)
- *Bias parameters*, constant or slowly varying (e.g., planetary mass)
- *Stochastic parameters*, modelled with random variations (e.g., noise effects)

The process also accounts for *consider parameters*, whose uncertainties are factored into the solution without direct estimation.

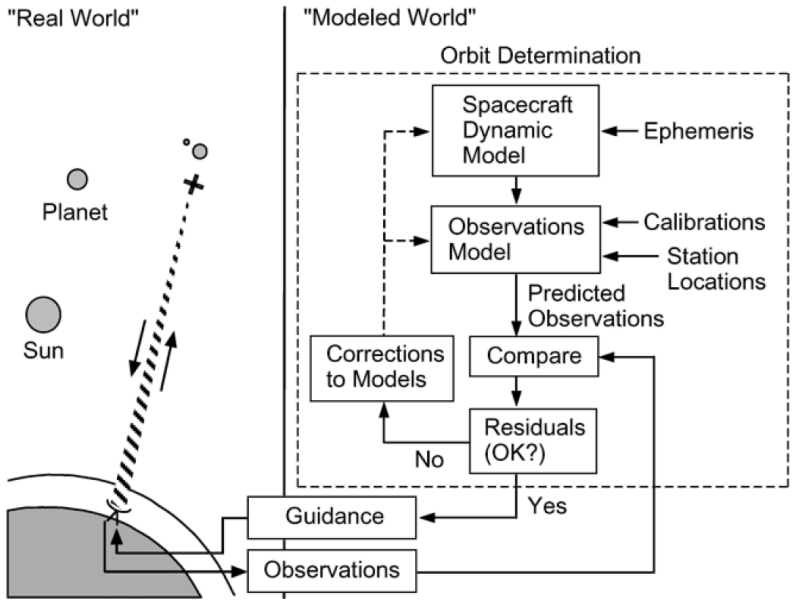

Figure 1.3: General scheme of the Orbit Determination process [2]

The orbit determination process is used for both mission operations, like the real-time navigation of a deep space probe, and also for science purposes. While in the first case, the main goal is to derive the spacecraft state at a specific time, in the second, the filter is used to derive many other parameters using the available data. For example, using radiometric measurements, the gravity field of interplanetary objects can be evaluated with high precision.

Radiometric measurements are the most common type of data used in the orbit determination process and are obtained through radio-link between the probe and Earth's ground stations. This classification comprehends *range* and *Doppler* measurements. These types of data, together with the estimation filter, are used to uniquely determine the state of a deep space probe with very high precision.

1.3 MONTE Python library

The Mission Operations and Navigation Toolkit Environment (MONTE) is an advanced Python library developed by NASA's Jet Propulsion Laboratory (JPL) to address the complex challenges of astrodynamics and space mission design. The platform is designed to support all phases of mission operations, from early-stage conceptual design to real-time navigation during flight. It provides a robust framework for a wide range of astrodynamic computations, enabling mission analysts and engineers to model spacecraft trajectories, optimize mission plans, and execute precise manoeuvres.

The software includes a comprehensive orbit determination system capable of processing measurements using stochastic models, covariance estimation and estimation filters. It supports the simulation and analysis of several measurement types, from ground-based tracking data to optical data. Furthermore, MONTE supports sensitivity analyses, enabling users to evaluate the impact of uncertainties on mission performance, as well as numerical integration methods for trajectory modelling.

MONTE has its roots in JPL's earlier navigation programs, including the "Single precision orbit determination program" in the 1960s and the "Double precision trajectory and orbit determination program" developed in the 1970s [18]. These programs supported key missions such as Ranger, Mariner, Voyager, and Cassini. The development of MONTE began in 1998 as part of an effort to modernize these systems by translating legacy navigation algorithms into a more maintainable and extensible C++/Python platform. It became operational in 2007, debuting on the Mars Phoenix mission, and by 2012, it was adopted as the primary navigation tool at JPL.

Chapter 2

Observational model

2.1 Pre-processing of radiometric measurements

The first step to evaluate the quality of the computed observables, i.e. the measurements produced by the model implemented with MONTE, is to archive and handle the available raw measurements. The collection of Doppler and Range measurements relies on the ground stations of both NASA's Deep Space Network (DSN) and ESA's ESTRACK and were used by the navigation team of Rosetta in 2014 to accomplish their operations. The radioscience laboratory of Forlì already possesses the data, which can also be freely downloaded from NASA's Planetary Data System and in particular in its "Small body node" which specializes in the archiving, cataloguing, and distributing of scientific data sets relevant to asteroids, comets and interplanetary dust [19].

The spacecraft *range observalbe* represents the distance of the S/C with respect to the transmitting G/S. It is determined by measuring the round-trip time of a ranging signal sent from a G/S. The signal consists of sinusoidal tones modulated onto the carrier. The spacecraft receiver locks onto this signal through a Phase-Locked Loop (PLL), producing a reference signal that helps demodulate the ranging signal. This signal is then filtered and modulated onto the downlink carrier. At the receiving station, another PLL creates a reference signal to demodulate the downlink one. The received range code is compared to a model of the transmitted code to calculate the round-trip light time [2].

The *Doppler observable* can be defined starting from the range. Indeed, the range can be approximated with

$$\rho = \tau_g c \tag{2.1}$$

wiht τ_g, the one-way light time and c the speed of light. Then, considering a constant frequency f_T of a signal transmitted by the S/C, the frequency received by the G/S is approximately defined as

$$f_R = \left(1 - \frac{\dot{\rho}}{c}\right) f_T \tag{2.2}$$

Being $\dot{\rho}$ the instantaneous range rate, the quantity $\frac{\dot{\rho}}{c} f_T$ represents the *Doppler shift* of the signal. Therefore, the Doppler measurement provides information on the

S/C's range rate with respect to the receiving station.

Radiometric data provided by ESA are called *IFMS measurements*. These are ASCII format texts generated and processed by ESTRACK stations. The IFMS data inherits its name from the equipment in charge of their generation: the *Intermediate Frequency Modulation System*. Each of these files is related to a different kind of data. This means that there can be several types of IFMS files:

- *Doppler measurements* that can be extracted at 1000, 100, 10, 1 or 0.1 sample per second; their data record contains the sample number and time, the unwrapped phase and the accumulated phase with respect to a reference.
- *Gain records* containing sample number and time, carrier level and polarization angle
- *Range measurements* can be extracted every 1 to 120 seconds (in user selectable increments of 1 second) delivering sample number and time, round trip delay modulo the ranging code, current code number and several flags and status words
- *Meteorological records* providing sample number and time, humidity, pressure and temperature at the ground station

Anyway, these files share a common structure that includes [20]:

- a *header* which contains information valid for the whole tracking pass, i.e. for each of the single sample provided within the file, such as station and spacecraft identifiers, time tags of first and last samples, total number of samples and several flags or other markers to identify the data
- the *measurement data*, i.e. the list of measurements collected during the tracking pass

In the case of IFMS files, each raw measurement is provided with one or more *calibration files* that are generated either before (pre-calibration) or after (post-calibration) each tracking pass. Such calibrations are particularly relevant for range observables because they allow us to estimate the station delay, i.e. the delay affecting the signal both in uplink and downlink because transmitting/receiving electronics and tracking reference point do not coincide. Since this quantity depends on their configuration, ground stations are equipped with a *group delay calibration system* able to measure this delay. Its output product is indeed the calibration file that must be used to correct ranging raw measurements. Without this correction, range measurements would be affected by a large and time-dependent bias error.

The radiometric measurements provided by the DSN are instead called *Tracking Data Message (TDM)* files, which are ASCII format texts as well. Also, in this case, the files are written with the *header-data list* structure. However, TDM files store all types of data together without generating a message for each of them. Similarly, station delay calibrations are provided within the TDM file itself. The *header* gives just some general information that identifies the basic parameter of the message, like

the date of creation, the version of the TDM and the provider (DSN). In addition, there will be several sub-headers called *metadata sections* [21], which support the knowledge of *data sections* (i.e. the list of actual measurements) by listing all those features needed to understand the data list.

The pre-processing procedure consists in several actions aiming to make the raw radiometric measurements usable by the MONTE library. Moreover, the pre-processing involves the adjustment of some features of the measurements based on what their use will be.

The activities conducted for this work are the following:

1. Load the raw data and archive the files according to the type of file (TDM or IFMS), content (Doppler or range) and time (year, month, day).

2. Conversion of IFMS and TDM files in the so-called *Binary Object Archive (BOA) format*. BOA files are databases of named objects, i.e. lists of information that can be retrieved using some type of identifier, that MONTE can read and handle [22]. These files are in binary form, making them much lighter but not user-readable without the necessary tools at hand. It is important to point out, that IFMS ranging measurements must be converted together with their calibration file.

3. Edit *Doppler measurements' count time*, increasing it to a value convenient for the usage that will be made. On one hand, increasing Doppler count time means mitigating the signal noise, on the other hand, the dynamical phenomena with time scales shorter than the count time won't be observed.

4. Edit *ranging measurements' sample time* to reduce the amount of data to be processed.

5. The pre-processed measurements that are used within the analysis are merged into a single BOA file.

2.2 Media calibrations

Electromagnetic waves interact with the medium in a variety of ways, changing the properties of the wave itself. The sources of these variations can be either:

- *dispersive*, meaning that the variations they induce depend on the signal's frequency

- *non-dispersive*, i.e. the variations remain the same for any signal frequency

These sources of error affect the quality of the measurements in terms of noise and delay accumulated by the signal. The noise affects mainly Doppler measurements while the delay is more important for range measurements. To be more precise, they make the signal gain:

- *phase delay*, i.e. the time delay of individual frequency components

- *group delay*, i.e. the time delay accumulated by the whole modulation of the signal

Focusing on Doppler measurements, they are particularly sensitive to noise [23], which increases their uncertainty. However, it is possible to improve the precision of measurements, by calibrating the noise accumulated by the signal in ionosphere and troposphere.

For ionospheric calibrations, the DSN provides the so-called *gimcal* files, which are GNSS-based corrections given in terms of a normalized polynomial for each tracking pass and their period is from spacecraft rise to set at the receiving station complex [24]. *Gimcal* files include calibrations for both DNS's and ESTRACK's stations.

Concerning tropospheric corrections, a first-order calibration is accomplished with seasonal models which do not depend on time and thus need to be delivered only once. The provided corrections represent the one-way zenith wet and dry delays, in meters, as Fourier series calibrations. These seasonal models are valid, again, for both DSN's and ESTRACK's stations. For a more accurate correction, the DSN also provide GNSS-based tropospheric calibration for both dry and wet components in the form of *ATC* files. They are provided as normalized polynomials that add to the just mentioned seasonal models. To a large degree, the troposphere can be considered azimuthally symmetric and therefore both corrections are given with respect to the zenith and can be calculated for any other direction using mapping functions. As an example, Niell's mapping function is a commonly used one

$$m(E,a,b,c) = \frac{1+\frac{a}{1+\frac{b}{1+c}}}{\sin E+\frac{a}{\sin E+\frac{b}{\sin E+c}}} \tag{2.3}$$

where E is the elevation angle, while a, b and c are coefficients depending on the receiver geographic location and measurement time. *ATC* files are provided only for DSN's stations.

For ESTRACK's stations, tropospheric calibration can be pursued through *IFMS Metereological data*

In Figure 2.1, an approximated noise budget for the Rosetta Doppler is shown, which has been computed using the reconstructed trajectory of the S/C published by ESA:

- The *plasma* curve includes the effects of both interplanetary and ionospheric plasma. The frequency shift is modelled as a function of the Sun-Earth-probe angle, which is valid whenever the spacecraft is at distances greater than 1 AU.

- The *troposhere's wet component* is modelled as a sinusoid with 1 year period, superimposed to an average value, having the maximum on the summer solstice and minima on the winter solstice.

- The *ground station* noise is obtained as a constant for 60 seconds count time Doppler, then scaled for any count time. Such constant takes into account the

contribution of all stations involved and depends on several factors such as wind buffeting, thermal deformations and gravity.

- The *spacecraft* contribution to Doppler noise depends on the design of its telecommunication system, particularly on the transponder. As a first-order approximation, it can be considered as constant.

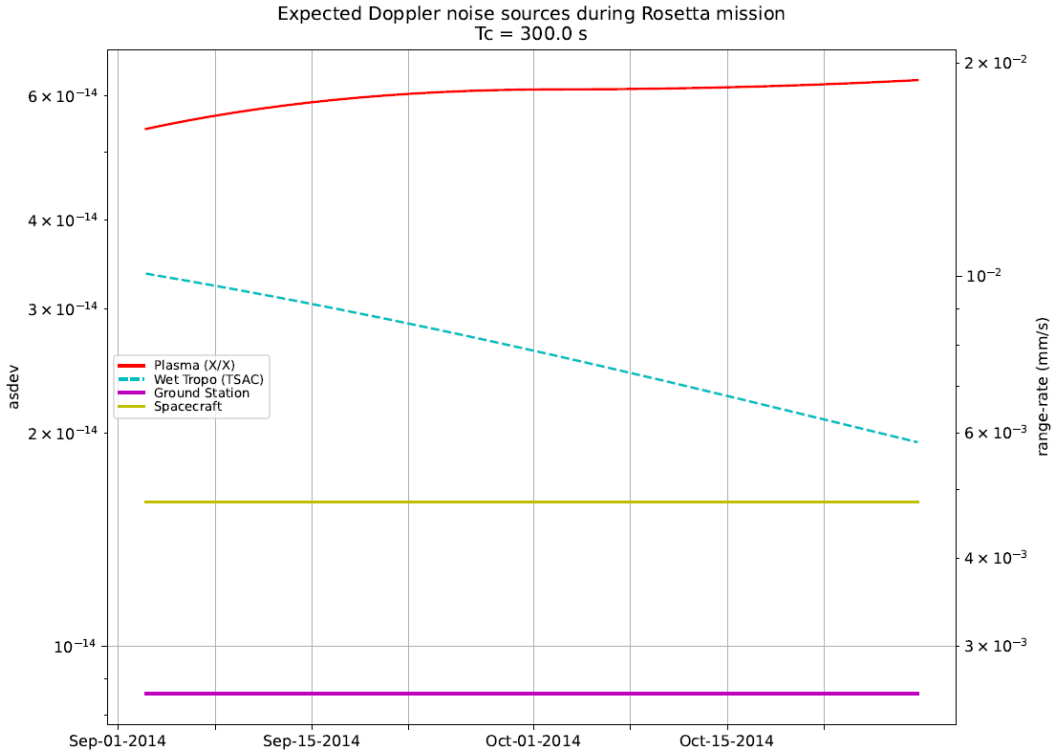

Figure 2.1: Rosetta mission expected noise during the period covered in the paper of Godard [3]

2.3 Reconstructed trajectories of Rosetta and 67P and planetary ephemeris

Being Rosetta a completed mission, the reconstructed heliocentric trajectories in EME2000 of both S/C and comet can be downloaded from one of the databases published by ESA and NASA.

These particular files, together with many others, can be found in NASA's Navigation and Ancillary Information Facility (NAIF) [25]. The NAIF team is dedicated to the issues of producing high precision, clearly documented and readily used *ancillary information* required by space scientists and engineers, about every space mission handled by NASA or with which NASA is involved; like in the case of Rosetta. To do so, NAIF has developed an information system called Spacecraft, Planet, Instrument, C-matrix, Events (SPICE) of which primary data sets are called

kernels or *kernel files*. These files are composed of navigation and other ancillary information providing precision observation geometry for use by the planetary science and engineering communities.

Indeed, the heliocentric trajectories of spacecraft and comet are published on NAIF as kernel files. In particular, they can be found among the so-called *spacecraft kernels (spk)*, i.e. the files concerning spacecraft, planets and other bodies ephemeris. The files used in this thesis work are: `RORB_DV_257_03___T19_00345.BSP` for Rosetta spacecraft and `CORB_DV_257_03___T19_00345.BSP` for 67P.

Moreover, also the planetary ephemeris are to be known. For instance, the position of Earth in the solar system is vital for the observables generation, together with its rotation that must be very precisely modelled. The ephemeris version used in this work is the JPL's DE405 ephemeris. Even if such a version is not the most updated, the *spk* files mentioned above are generated using this specific set of ephemeris. Therefore, for consistency reasons, it is important to use the same version of ephemeris.

2.4 High-gain antenna modelling

2.4.1 Rosetta communication system overview

Communication for Tracking, Telemetry, and Command (TTC) with Earth throughout the entire Rosetta mission is ensured by a combination of three antenna systems, used at different stages of the mission, along with various electrical units carrying out specific tasks. The telecommunication subsystem is designed to interface with the ESA ground segment during normal operations and with the NASA Deep Space Network in emergencies [26]. The three antenna systems are::

- Two Low Gain Antennas (LGAs) providing a quasi omnidirectional coverage, which can be used in the near-Earth mission phase at S-band for telemetry uplink and downlink or, most importantly, for telecommand uplink at S-band for emergencies with Earth to probe distance up to 6.5 AU
- Two Medium Gain Antennas (MGAs) ensure default emergency uplink and downlink communication once the spacecraft has entered Sun-pointing mode. The S-Band MGA is a flat patch antenna, while the X-Band MGA is an offset-type 0.31-meter reflector antenna. The MGAs also support certain mission communication functions during various phases of their operational lifetime, thanks to their significantly larger coverage area.
- A 2.2 meters cassegrain High Gain Antenna (HGA) providing primary communication during the whole mission in S- and X-band both in uplink and downlink.

The S/C should be able to autonomously point the HGA toward Earth by utilizing star sensor attitude data and an onboard stored ephemeris table. The last feature implies the need for an autonomous pointing mechanism of the HGA, which corresponds to a *steerable HGA*.

The Antenna Pointing Mechanism (APM) is a two-axis system that allows the HGA to move in both azimuth and elevation. Control is managed by the attitude, orbit control and monitoring subsystem, which always knows the spacecraft's orientation and Earth's direction, enabling it to determine the necessary antenna positioning. Positioning commands are sent from the attitude control subsystem's interface unit to the APM's electronics, which then routes them to the actuators. The HGA's elevation movement is physically limited to +30°/-165° from its reference position after deployment. Before and during deployment, the range extends to -207°/+30°. The azimuth movement is limited to +80°/-260° from its reference position. In Figure 2.2 it can be visualized how the HGA can be steered.

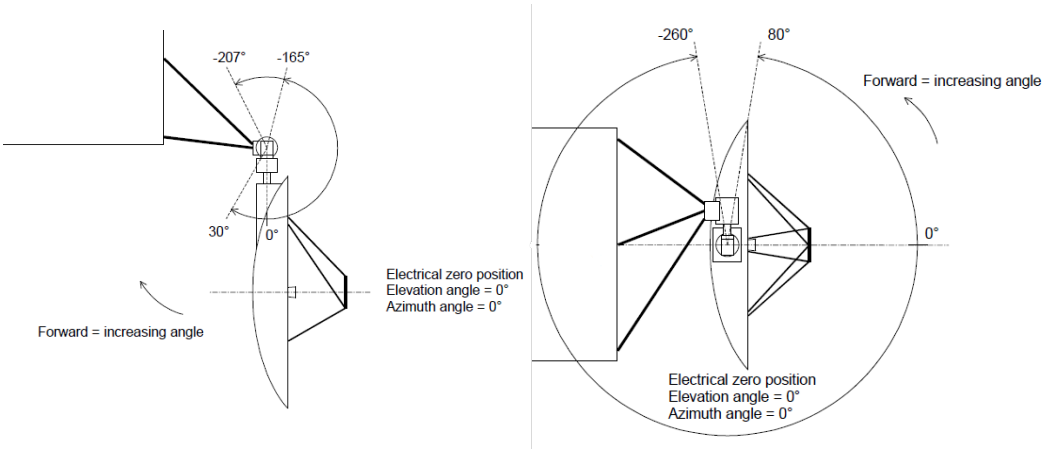

Figure 2.2: High Gain Antenna Pointing Mechanism elevation (left) and azimuth (right) angles [4]

To make the generation of Doppler observables more reliable, the model of Rosetta computed in MONTE must be able to use the centre of the HGA's disc as a reference point for all signals transmitted and received by the S/C. By doing this, it is assumed that all the uploaded raw measurements are transmitted and received by the HGA, although they could also be linked to the LGAs or MGAs. This assumption is quite reasonable since the residuals are computed only from X/X links, i.e. the LGAs can be discarded. On the other hand, the MGAs are possible candidates for the measurements generation, but even if they are used, the amount of measurements from the HGA would be far greater and so, this imperfection of the model won't affect the final results.

2.4.2 Spacecraft and HGA reference frames

To model the HGA movements, it is necessary to understand the definitions of Rosetta's frames used to locate the HGA centre. A detailed description of all the frames involved in the mission is provided in Rosetta's *frame kernel (fk)* [17], which also hosts the actual SPICE information content about its frames.

Starting from the spacecraft frame, the HGA orientation is described using three different frames, the first two are time-varying while the last is a constant offset. The details are deeply explained inside the user manual "*Coordinate Systems For Rosetta*" [5]. The first frame is the one associated with the elevation angle and can

be called *HGA elevation frame* and accounts for the definitions of "elevation axis" and "azimuth axis" shown in Figure 2.3:

- +Y axis along the elevation axis of the APM, in the same direction as the spacecraft Y-axis
- +Z axis along the projection of the azimuth axis onto the plane perpendicular to the elevation axis pointing to the spacecraft centre
- +X axis completes the right-handed frame
- The origin of this frame is the gimbal of the APM
- its reference frame is the S/C body frame

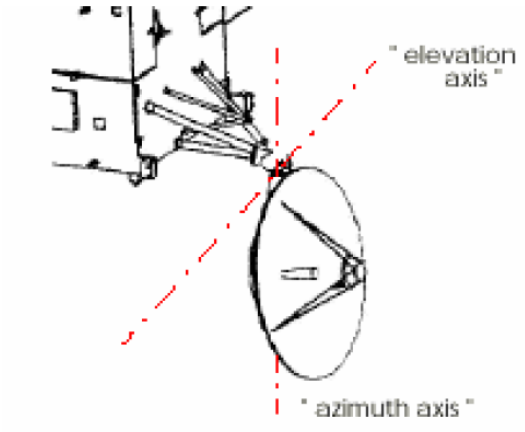

Figure 2.3: Definition of "*elevation axis*" and "*azimuth axis*" [5]. They are the axes of rotations defining the two angles respectively, azimuth axis changes its orientation depending on the elevation axis

The second frame refers to the motion in terms of azimuth angle and is referred to as *HGA azimuth frame*:

- +X axis is parallel to the direction of the antenna's boresight
- +Z axis along the azimuth axis pointing to the spacecraft centre
- +Y axis completes the right-handed frame
- The origin of this frame is the gimbal of the APM
- its reference frame is the HGA elevation frame

The final frame, called *HGA frame* is simply a +90 degrees offset of the HGA azimuth frame on its Y-axis and the origin is at the centre of the antenna's dish.

All of these frames, have to be defined inside the MONTE setup. On one hand, the HGA frame must be precisely specified as an offset frame rotating HGA azimuth frame of 90 degrees about the Y-axis. On the other hand, the time-varying frames' orientation is supplied by another type of kernel file: the *C-matrix kernels (ck)*. In general, *ck* files provide time-tagged pointing angles and angular rates for the spacecraft bus and its components.

Indeed, for this particular case, two *ck* files are needed:

1. one for the spacecraft bus attitude with respect to EME2000 (`ROS_SC_REC_V01.BC`)
2. one containing both the orientations of HGA elevation frame and azimuth frame (`ROS_HGA_2014_V0045.BC`)

2.4.3 Centre of gravity and spacecraft components distance offsets

An important consideration to keep in mind is that the heliocentric trajectory provided in NAIF is referred to the probe's centre of mass. On the other hand, the position of the HGA dish centre is defined through a chain of reference frames that starts from the spacecraft frame origin. The chain of relative positions that must be computed is

$$\textit{Centre of gravity} \rightarrow \textit{S/C body frame origin} \rightarrow \textit{HGA gimbal} \rightarrow \textit{HGA dish centre}$$

These distance offsets are provided in the form of *spk* files (as the trajectories) and can also be downloaded from NAIF. More precisely, the kernels needed for this task are two:

1. an *spk* file providing the offset between the launch vehicle interface point and the centre of gravity (`ROS_COG_V4.BSP`)
2. an *spk* file containing all the offsets among the components of the spacecraft (`ROS_STRUCT_V8.BSP`)

The position of the centre of gravity is not constant over time and varies throughout the mission for several reasons, namely the fuel consumption and its displacements during manoeuvres, the detachment of the lander Philae or the movement of articulations. For this reason, the centre of gravity position in the body frame is described as a set of time-tagged values generated every 5 minutes. The values are given in the spacecraft frame with origin in the centre of mass, therefore `ROS_COG_V4.BSP` provides the position of the launch vehicle interface point with respect to the centre of gravity.

On the contrary, the locations of Rosetta's components, such as the HGA gimbal, have fixed distances. Accordingly, they are given once for the entire mission. It is important to note that this is true also for articulated parts of the spacecraft. Taking as an example the steerable HGA, the dish centre location can be uniquely defined with the combination of the HGA frame, plus the constant distance offset existing between the gimbal and the dish centre. Meaning that its relative position time-variation is due to the changing orientation of the frame and not to distance offset variations.

2.5 Ground station bias and spacecraft transponder delay estimation

While, the implementation of the HGA particularly improves the generation of Doppler observables, the main effect to take into account for range measurements are delays. In particular, there are two important types of delays that have to be removed:

- The transponder group delay leads to a constant bias on the range measurements. Actually, this delay slowly shifts in time due to hardware degradation, but such variation is negligible. For the transponder delay a value of 2.152 microseconds is assigned (number provided by Rosetta's navigation team).
- The ground station biases are instead time-dependent delays. They change in time, are unique for each station and depend on several variables that would be difficult to model, such as the room temperature and humidity at the receiver and meteorological conditions. The only way to get rid of them is through their estimation. The station delays are initially set at 0 seconds. Being them time dependent, one measurement bias must be defined for each tracking pass of each station.

Moreover, the exact value of the S/C's transponder bias is also estimated to account for variations due to the degradation of the telecommunication subsystem.

2.6 Observational model validation

In Figure 2.4, the Doppler residuals prior passthrough process are shown. From the second plot, displaying a shorter timespan, it is clear that the residuals show signatures of about 0.5 mm/s. The reason for such signatures is due to the unmodelled Rosetta's High Gain Antenna (see Section 2.4).

In Figure 2.5 instead, the range residuals before the passthrough process are displayed. In this plot, the previously mentioned missing biases can be recognized. The transponder group delay moves all residuals far from zero, while station biases are visible from the not constant displacement of the residuals over time.

From Figure 2.6, it can be noted that the doppler residuals have largely improved after the passthrough process. The introduction of the steerable HGA made them lose the previously mentioned signatures. With the kernels integrated into the setup, also the statistics are better and are very close to the values of the reference paper. Indeed, it is possible to notice that the final residuals' mean value is very close to zero and the Root Mean Square (RMS) of 0.05052 mm/sec is similar to the one obtained by Rosetta's navigation team, even if slightly larger. One possible reason for this difference can be the different number of samples. Indeed, the total number of measurements is 12249 against the 10662 samples used by Godard et.al [3]. Their data post-processing may have been more aggressive in terms of outliers cutting, leading to both a smaller number of samples and lower RMS value.

About ranging, the final residuals are as good as the Doppler ones. Indeed, Figure 2.7 shows that statistics satisfactorily match those of the reference paper.

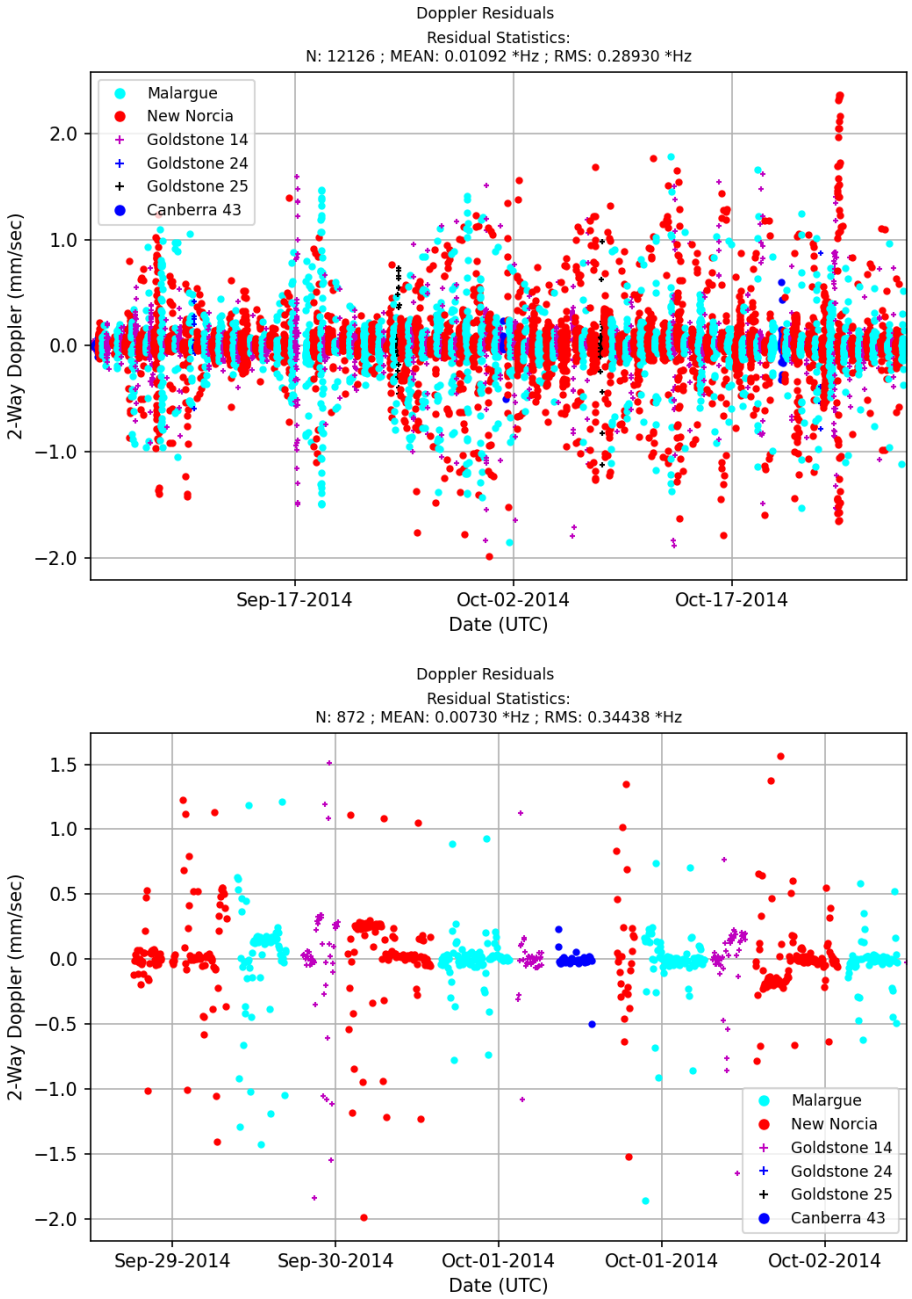

Figure 2.4: 300 seconds count time Doppler observables' residuals of the arc analysed in [3]. In the second picture, the signatures due to the missing modelling of the HGA are clear

The transponder and station biases have been correctly estimated since the residuals are all close to zero and no signatures are present.

The final residuals have been obtained with

- 300 seconds count time for Doppler residuals

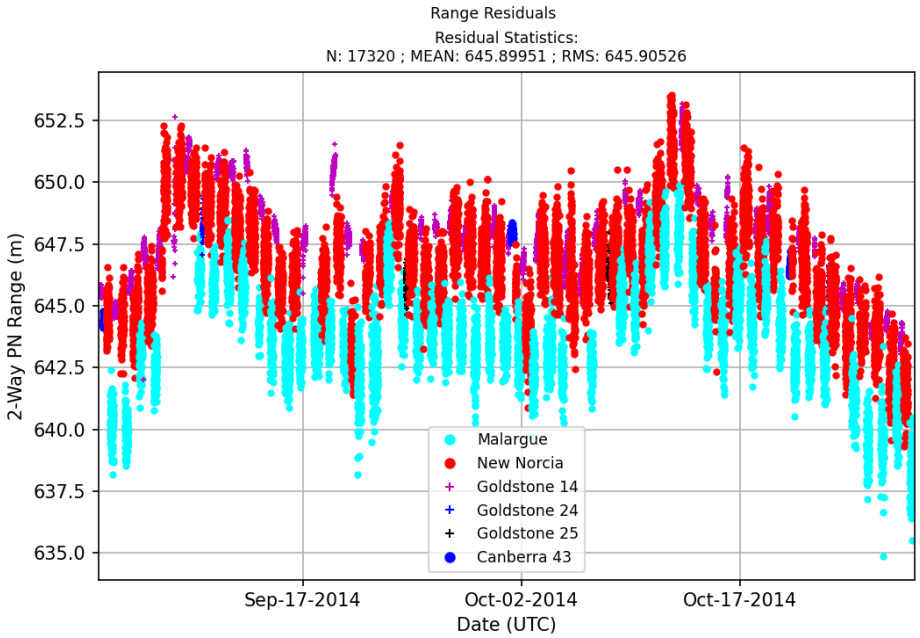

Figure 2.5: Ranging observables' residuals of the arc analysed in [3] with 200 seconds sampling time. It is clear that important delays are missing

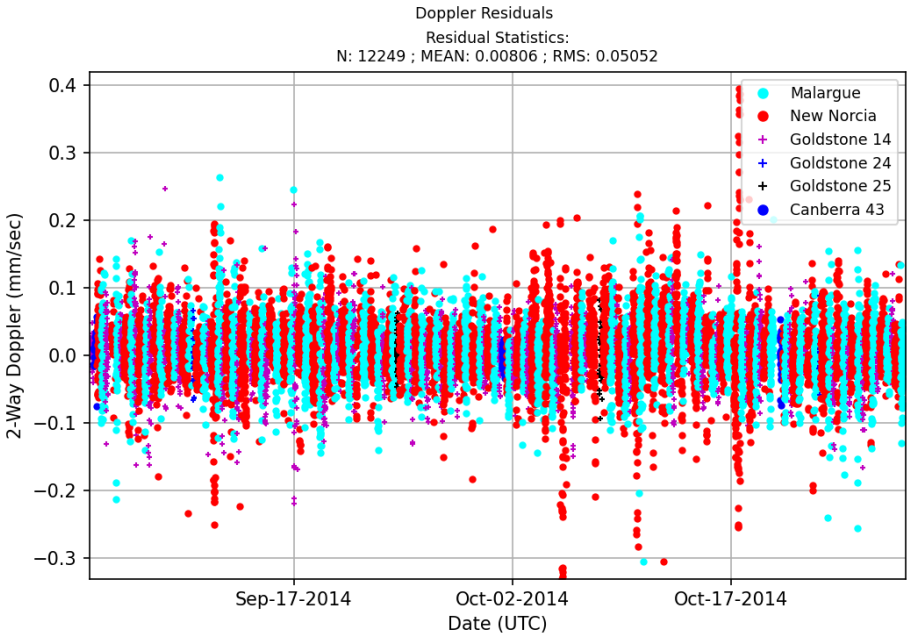

Figure 2.6: Doppler residuals after passthrough process

- 200 seconds sample time for DSN range residuals
- 2500 seconds sample time for ESTRACK range residuals

The numbers are chosen to match the results of Godard et.al and make a

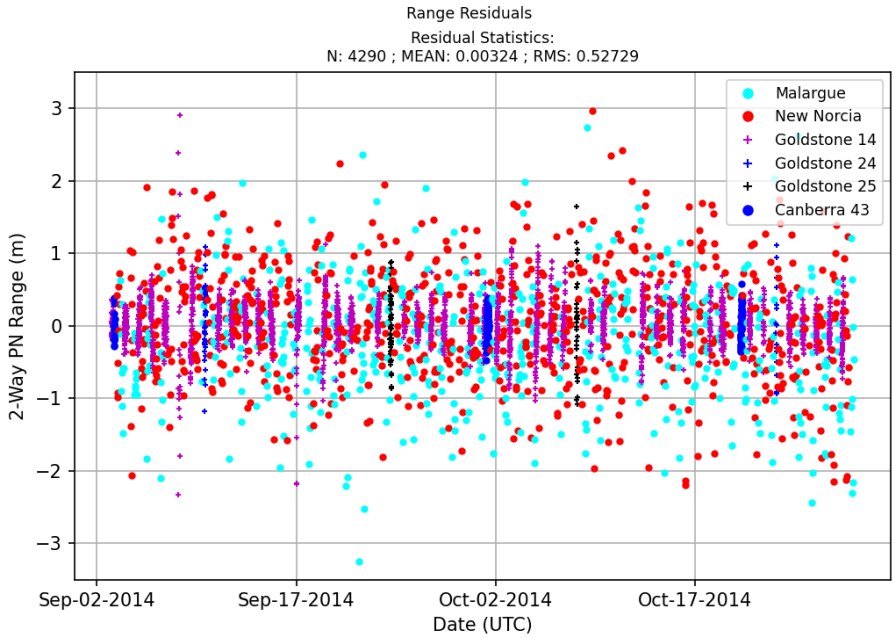

Figure 2.7: Range residuals after passthrough process

comparison which proves the effectiveness of the passthrough.

To confirm the correct estimation of the ground station biases, an additional plot is displayed in Figure 2.8. Such a plot shows the value of the bias estimated by the filter for each ground station and for each tracking pass and, once again, it satisfactorily matches the results of the reference paper.

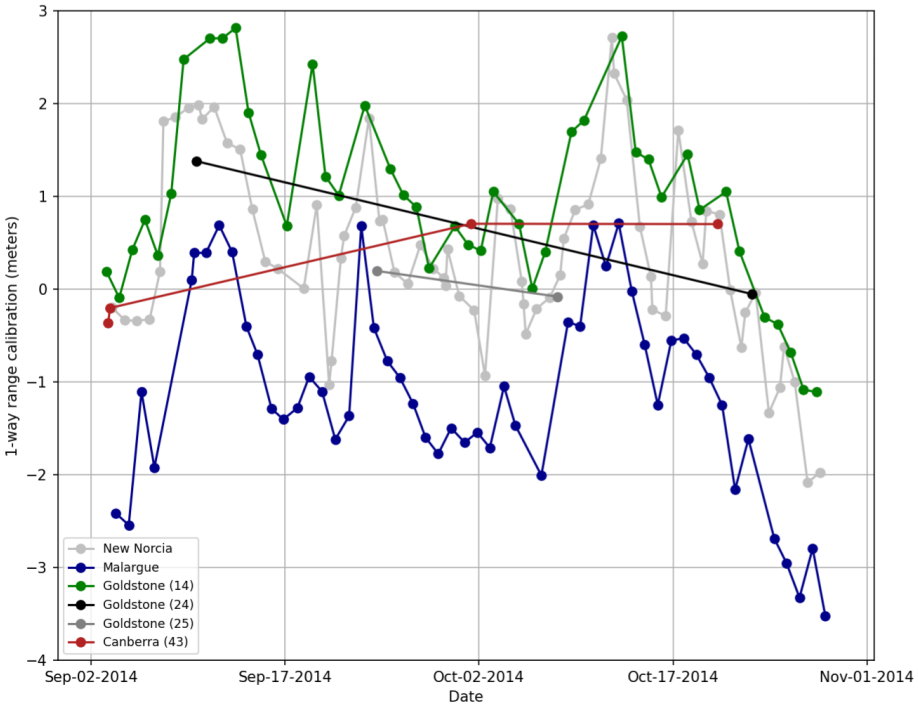

Figure 2.8: Estimated values of Ground Stations' biases for each station and tracking pass.

Chapter 3

Dynamical model

3.1 Main forces acting on Rosetta spacecraft

The most important forces in the pre-lander delivery phase scenario are the following:

- gravity of 67P
- gravity perturbations from Sun and planets
- Solar Radiation Pressure (SRP)
- coma drag

An evaluation of these forces' order of magnitude can be carried out using the reference trajectory published on NAIF and obtaining their values from analytical models. By performing this operation, the plot in Figure 3.1 can be computed.

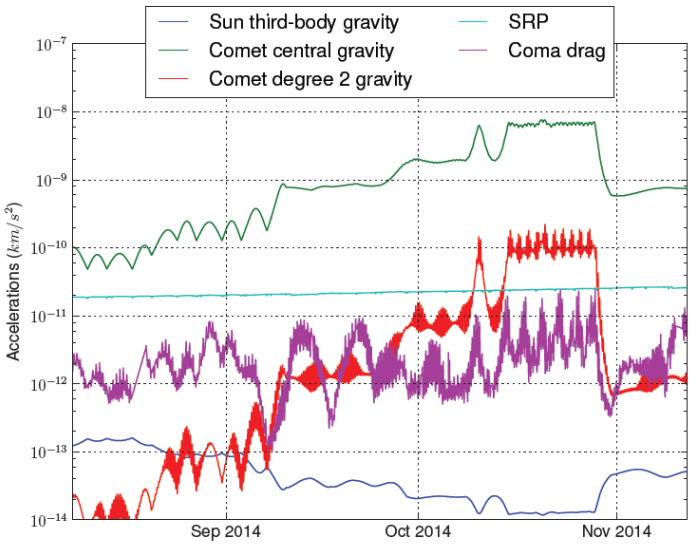

Figure 3.1: Time evolution of the accelerations affecting Rosetta's dynamics

It is possible to see that the strongest force acting on Rosetta is 67P's gravity changing over time due to relative position variations between S/C and comet. Also,

the SRP contributes significantly, with an acceleration remaining approximately constant over time. Coma drag and second-order gravity of the comet are approximately in the same order, while the Sun's gravity perturbation has the weaker contribution for most of the pre-lander delivery phase.

3.2 Gravity

During the pre-lander delivery phase, Rosetta was orbiting close to the comet. Therefore, the main gravity source was 67P. In particular, this is true whenever the S/C is within the comet's Sphere of Influence (SOI) with respect to the Sun, which can be calculated using the formula:

$$r_{SOI} = \rho \left(\frac{m_{comet}}{m_{Sun}} \right)^{2/5} \tag{3.1}$$

where ρ is the distance between 67P and the Sun and m_{comet} and m_{Sun} are the masses of 67P and the Sun respectively. Taking the average comet-Sun distance over the studied period, the value obtained to define 67P's SOI is 62 km and the S/C is indeed within this distance for most of the pre-lander delivery phase.

Referring to the results obtained by Godard et.al. [3], the values of the comet's gravitational parameter and spherical harmonics coefficients are listed in Table 3.1. Using these parameters and defining a normalization radius, in this case of 1 km, MONTE can directly provide the accelerations generated by the comet's gravity field using a built-in algorithm.

Table 3.1: Gravitational Parameter and Spherical Harmonics Coefficients of comet 67P Churyumov Gerasimenko [3]

Parameter	Value
GM $[km^3/s^2]$	6.665×10^{-7}
C20	-5.54×10^{-1}
C22	2.03×10^{-1}
S22	-8.18×10^{-3}
C30	-3.8×10^{-1}
C31	-1.42×10^{-1}
S31	1.1×10^{-1}
C32	6.1×10^{-2}
S32	-2.7×10^{-2}
C33	8×10^{-3}
S33	-5×10^{-2}

Other than the comet's one, the dynamical model takes into account also for the gravity of Sun, planets, Moon and Pluto. All of them are modelled as point-masses, with the exception of the Sun, of which J2 contribution is also taken in consideration. For each of them, relativistic corrections are applied.

3.3 Solar radiation pressure

One of the most important parameters that define the SRP is the cross-sectional area exposed to the Sun by the S/C. To model such parameter, the following surface elements have been implemented for the Rosetta S/C:

- Six rectangular surfaces for the Bus. Their orientations are assigned using the S/C body frame. In particular
  - ±X Bus Sides of area 4.2 m^2
  - ±Y Bus Sides of area 5.6 m^2
  - ±Z Bus Sides of area 5.88 m^2
- the HGA dish with 1.1 meters radius and 0.344 meters depth, normally oriented as the +X axis of the HGA frame, which has been defined in detail in Section 2.4.2.
- two rectangular surfaces of 32 m^2 to reproduce the solar panels oriented according to the SA ±Y frames explained below.

To express the orientation of the solar panels, it is necessary to follow a procedure similar to the one carried out for the HGA. Indeed, the orientation evolution of the S/C body frame has already been implemented by using the *ck* file `ROS_SC_REC_V01.BC`. Then starting from the body frame, two chains of reference frames must be computed (one for each solar panel). First of all, the frames giving the Solar Arrays (SA) reference orientation must be defined. These frames are fixed and called *SA +Y_0 frame* and *SA -Y_0 frame* for the SA on the S/C +Y and -Y side respectively. They are defined as follows:

- +Z axis is co-aligned with the +X axis of the S/C body frame
- +Y axis is oriented towards the S/C bus. i.e. it is positively oriented from the SA tip towards the gimbal
- +X axis completes the right-handed frame
- the centre corresponds to the location of the SA gimbal

The gimbal can rotate the arrays about the +Y axis. Then, as for the HGA azimuth and elevation frames, the actual orientation of the SAs must be retrieved from a *ck* file called `ROS_SA_2014_V00048.BC`. This kernel contains the time-changing orientation of SA ±Y frames with respect to SA ±Y_0 ones.

Other than the size and orientations of the shapes composing Rosetta, their optical coefficients are equally important to model the interaction of the S/C with the solar radiation. Therefore, the thermal-optical properties of the surfaces, have been taken from the work of Kato et.al [6], "*Precise modelling of solar and thermal accelerations on Rosetta*", and are listed in Table 3.2. The shown coefficients refer to the following formula for the acceleration of a surface element dA due to SRP:

$$\vec{a}_{SRP} = -\frac{P}{mc}\left[(1-\gamma_s)\vec{r} + 2(\gamma_s \cos\theta + \frac{1}{3}\gamma_d)\vec{n}\right]\cos\theta dA \tag{3.2}$$

where P is the incident radiative power, m is the mass of the S/C, c is the speed of light, $\vec{r}$ is the direction of the incoming light, $\vec{n}$ is the direction of the surface normal and θ is the angle between the two.

Table 3.2: Specular and diffuse reflectivity coefficients of Rosetta's surfaces

Surface	γ_s	γ_d
Bus	~ 0.0	0.07
Solar Array	0.141	0.016
HGA Front	0.01	0.06
HGA Back	0.01	0.06

It is important to note that *self-shadowing* is not implemented in this model. However, the surfaces of the bus are defined such that they activate only when their normal is facing the Sun. However, the shadow of Churyumov-Gerasimenko is taken into account.

Before using the implemented SRP model in trajectory integrations, it is fundamental to test it and confirm its trustworthiness. This task can be carried out through the reference trajectories provided in NAIF. Once the SRP model is loaded in the setup, it is sufficient to evaluate the computed acceleration and plot it over time. The values obtained from the model satisfactorily match the ones published by Kato et.al [6], as can be observed in Figure 3.2.

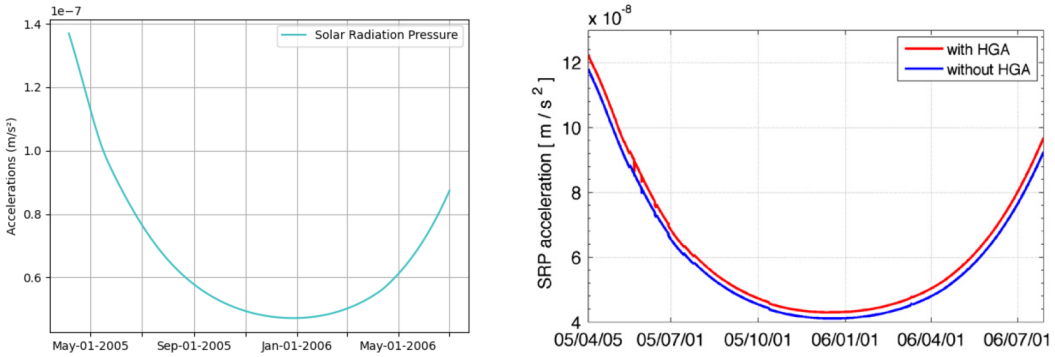

Figure 3.2: Comparison between SRP acceleration on Rosetta obtained from the model of this work (left) and the results of Kato et.al [6] (right)

3.4 Coma drag

Comets are small celestial objects made up of a combination of ice and dust. As a comet gets closer to the Sun, the heat causes the ice to sublimate, turning it directly into gas. This gas carries dust particles away from the comet's surface, forming a cloud-like atmosphere around the comet known as the coma. Therefore, the coma is a mixture of gas and dust that extends for several kilometres around the nucleus. The comet's gravity is too weak to hold onto this atmosphere, allowing most of the particles to escape, except for a few larger ones.

In particular, other than dust, the coma of Churyumov-Gerasimenko is mainly composed of H_20, CO_2, CO, O_2. The activity of coma formation is not uniform across its surface and deeply depends on the illumination conditions [27].

The interaction between the coma and the spacecraft's surfaces leads to a drag effect inducing accelerations that, during the period close to perihelion, reach intensities comparable to the ones generated by the comet's gravity. Such accelerations develop torques as well, affecting also the attitude state of the probe [28].

3.4.1 Stochastic accelerations to evaluate coma drag

Due to its complexity, no coma drag model has been introduced within the dynamical setup. From Figure 3.1, it is possible to see that this acceleration is not negligible in this phase of the mission. If no model is introduced, the filter would try to use the available estimation parameters (like the manoeuvres) to try and compensate for the missing acceleration, leading to an unreliable estimation.

Therefore, the strategy chosen to take into account the un-modelled dynamics is through *stochastic accelerations*. In particular, a series of accelerations have been defined and assigned to the Rosetta S/C, each of which lasts 2 hours and is constant within that time. Then, their parameters have been added to the *solve-for* ones.

Furthermore, the coma is a phenomenon in which gas and dust particles are ejected from the comet's surface with velocities that can reach hundreds of meters per second. On the other hand, the S/C speed with respect to the comet is much lower (sub-meter per second). Therefore, the coma drag is a force mainly acting in the direction that goes from the comet toward the probe. For this reason, the frame in which the stochastic accelerations have been chosen to be defined is a Radial-Transversal-Normal (RTN) Frame with:

- X axis pointing from the comet's centre of mass to Rosetta's centre of mass
- Z axis aligned with the angular momentum of Rosetta's orbit around 67P
- Y axis to complete the right-handed frame

Stochastic accelerations are both a powerful and dangerous tool since they can absorb the missing dynamics that bring the residuals far from zero. At the same time, they can steal some information concerning the other parameters that are being estimated, affecting the estimation itself. Indeed, the goal is to keep them fewest possible while making them short enough to accurately model the dynamic that they must absorb. Thus, they have been chosen to be 2 hours long.

To produce a more realistic estimation of the coma drag and prevent the filter from divergence, a constraint has been added to the stochastic accelerations. Specifically, the constraint is formulated as

$$a_i|_{k+1} - a_i|_k < \sigma_a \times 10^{-3} \tag{3.3}$$

where $a_i|_k$ is the stochastic acceleration of the k-th batch and i-th estimation iteration, while σ_a is the uncertainty on the stochastic accelerations.

3.5 Manoeuvres

3.5.1 Propulsion subsystem overview

The propulsion system of the Rosetta spacecraft [4] uses a pressure-fed bipropellant setup with Monomethylhydrazine and Nitrogen Tetroxide. It can work in both regulated and blow-down modes, offering a ΔV of over 2100 m/s plus attitude control. It can operate in three-axis mode and spin-stabilized mode around the X-axis, as long as the spin rate stays below 1 rpm. This system has a high level of redundancy to meet the special needs of the mission.

Most components and pipes are installed on the S/C -X panel using brackets made of low thermal conductivity material. The system has 24 thrusters, each with 10 N of force, for controlling both attitude and orbit. The thrusters' configuration has been designed to provide pure forces and pure torques. They are paired on brackets, with one main and one backup thruster in each pair. The system can run up to 8 thrusters at the same time.

3.5.2 Orbital and desaturation manoeuvres modelling

Other than passive dynamics, Orbital Control Manoeuvres (OCM) and desaturation manoeuvres must be taken into account as well.

A priori values for the OCMs are provided by Godard et al. and are listed in Table 3.3. The precise time at which the manoeuvres are performed can be extracted from the OCM housekeeping data, which can be freely downloaded from the small body node [19]. Indeed, there are files showing the number of on/off cycles each thruster has gone through, associated with a precise time tag in universal Time Coordinated (UTC). Using such data, it was possible to generate plots as the one in Figure 3.3, which allows to immediately visualize whenever a manoeuvre was performed. By comparing the housekeeping data and the OCM list, it has been possible to conclude that orbital manoeuvres are the ones performed using simultaneous burns of thrusters 9, 10, 11 and 12. Moreover, the Rosetta science user guide for housekeeping engineering data [7] provides the table reproduced in Table 3.4, that lists the thruster coordinated and thrust direction cosines in the body frame of Rosetta. With such information, it was possible to conclude that all OCMs are directed along the Z body axis.

Table 3.3: List of OCM names, times and *a priori* values

Manoeuvre	Time (UTC)	ΔV [mm/s]
TGM-1	2014-09-03 09:00	565
TGM-2	2014-09-07 09:00	452
GMP-1	2014-09-10 09:00	193
GMP-SLOT-1	2014-09-14 09:00	25
GMP-2 (leg1)	2014-09-17 09:00	85
GMP-2 (leg2)	2014-09-03 10:30	88
GMP-SLOT-2	2014-09-21 09:00	19
GMP-3	2014-09-24 09:00	16
GMP-4	2014-09-29 09:00	106
GMP-SLOT-2.5	2014-10-01 11:35	14
GMP-SLOT-3	2014-10-05 09:10	10
COP-1	2014-10-08 09:00	37
COP-SLOT-1	2014-10-12 09:10	22
COP-2	2014-10-15 09:10	57
COP-SLOT-2	2014-10-19 09:00	12
COP-SLOT-3	2014-10-22 09:00	12
SDP-1	2014-10-28 13:00	82
SDP-2	2014-10-31 02:10	96

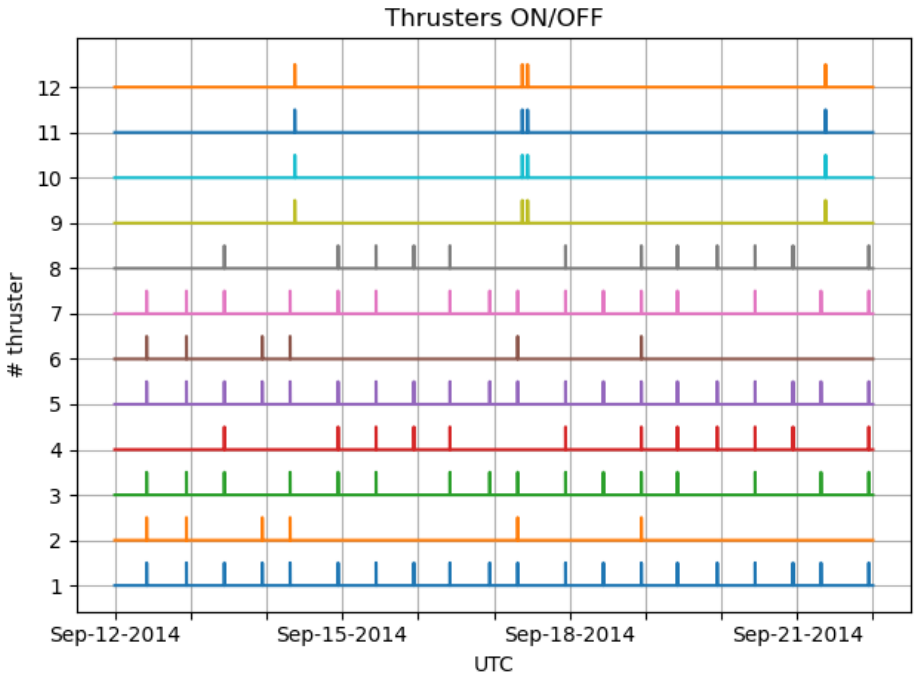

Figure 3.3: Thrusters state (ON/OFF) as a function of time

Table 3.4: Thruster Coordinates and thrust cosine directions in S/C's Body Frame [7]

Thruster	Coordinates in S/C Frame			Direction Cosines w.r.t S/C Frame			Thrust [N]
	X	Y	Z	X	Y	Z	
1A	-1231.9	-1139.5	2176.8	0.4698	0.8660	-0.1710	10
2A	1231.9	-1139.5	2176.8	-0.4698	0.8660	-0.1710	10
3A	-1231.9	-1139.5	-84.252	0.4698	0.8660	0.1710	10
4A	1231.9	-1139.5	-84.252	-0.4698	0.8660	0.1710	10
5A	-1231.9	1139.5	-84.252	0.4698	-0.8660	0.1710	10
6A	1231.9	1139.5	-84.252	-0.4698	-0.8660	0.1710	10
7A	-1231.9	1139.5	2176.8	0.4698	-0.8660	-0.1710	10
8A	1231.9	1139.5	2176.8	-0.4698	-0.8660	-0.1710	10
8A	-1160	-903	-199.2	0.0000	0.0000	1.0000	10
10A	1160	-903	-199.2	0.0000	0.0000	1.0000	10
11A	1160	903	-199.2	0.0000	0.0000	1.0000	10
12A	-1160	903	-199.2	0.0000	0.0000	1.0000	10
Thruster	Coordinates in S/C Frame			Direction Cosines w.r.t S/C Frame			Thrust
	X	Y	Z	X	Y	Z	
1B	-1238	-1150.9	2101.9	0.4698	0.8660	-0.1710	10
2B	1238	-1150.9	2101.9	-0.4698	0.8660	-0.1710	10
3B	-1238	-1150.9	-9.371	0.4698	0.8660	0.1710	10
4B	1238	-1150.9	-9.371	-0.4698	0.8660	0.1710	10
5B	-1238	1150.9	-9.371	0.4698	-0.8660	0.1710	10
6B	1238	1150.9	-9.371	-0.4698	-0.8660	0.1710	10
7B	-1238	1150.9	2101.9	0.4698	-0.8660	-0.1710	10
8B	1238	1150.9	2101.9	-0.4698	-0.8660	-0.1710	10
9B	-1160	-827	-199.2	0.0000	0.0000	1.0000	10
10B	1160	-827	-199.2	0.0000	0.0000	1.0000	10
11B	1160	827	-199.2	0.0000	0.0000	1.0000	10
12B	-1160	827	-199.2	0.0000	0.0000	1.0000	10

Chapter 4

Estimation filter

4.1 Estimation filter overview

The estimation filter is a fundamental tool for orbit determination and navigation. It is used to estimate parameters of a dynamical system, such as the state of a S/C, by processing sets of measurements collected over time. Hereafter, the key concepts of the estimation filter are briefly explained.

Dynamical model

The *state vector* $\mathbf{x}$ is the vector of *solve-for* parameters, i.e. the ones that need to be estimated. It includes both *dynamical parameters* $\mathbf{d}$, changing over time, and *bias parameters* $\mathbf{b}$, constant over time:

$$\mathbf{x} = \begin{bmatrix} \mathbf{d} \\ \mathbf{b} \end{bmatrix} \tag{4.1}$$

Examples of a dynamical parameter and a bias parameter are the state of the S/C and the mass of a celestial body respectively.

The dynamical model of a system can be described by a set of first-order differential equations which describe the state vector evolution:

$$\dot{\mathbf{x}}(t) = \mathbf{f}(\mathbf{x}(t), t), \quad \mathbf{x}(t_o) = \mathbf{x}_o \tag{4.2}$$

with $\mathbf{f}$ being a system of non-linear functions.

The dynamical model allows to propagate the state vector from an initial condition $\mathbf{x}_o$ to any time t. The solution to this differential equation is often referred to as the *integral flow*:

$$\mathbf{x}(t) = \boldsymbol{\varphi}(\mathbf{x}_o) \tag{4.3}$$

Therefore, the integral flow is a function that maps the solve-for parameters from a reference time t_0 to any other instant t.

From this concept, the *state transition matrix* can be introduced:

$$\boldsymbol{\Phi}(t, t_o) = \frac{\partial}{\partial \mathbf{x}(t_o)} \mathbf{x}(t) \tag{4.4}$$

This matrix carries the information on how variations in the initial conditions, affect the the state vector at any time t and it is used to linearize the system.

Measurements model

The observables are collected in the *measurements vector*. The *observed* measurements vector $\mathbf{z}$ contains the observables collected, while the *estimated* measurements vector $\hat{\mathbf{z}}$ represents the computed observables generated by means of the model:

$$\mathbf{z} = \Big[z_1, z_2, \cdots, z_m\Big]^T, \quad \hat{\mathbf{z}} = \Big[\hat{z}_1, \hat{z}_2, \cdots, \hat{z}_m\Big]^T \tag{4.5}$$

The relation between measurements vector and state vector is expressed as:

$$\mathbf{z} = \mathbf{g}(\mathbf{x}(t), t) + \boldsymbol{\nu} = \mathbf{g}(\mathbf{x}_0) + \boldsymbol{\nu} \tag{4.6}$$

where the integral flow has been expressed to show that measurements at any instant t depend only on the initial state of the system. Moreover, $\boldsymbol{\nu}$ is the *measurement noise vector*, whose elements are assumed to be gaussian random variables with zero mean. For this particular random variables, their Probability Density Function (PDF) is fully described by their variance:

$$E[\boldsymbol{\nu}] = \mathbf{0} \tag{4.7}$$

$$Cov[\boldsymbol{\nu}] = E[\boldsymbol{\nu}\boldsymbol{\nu}^T] = \boldsymbol{P}_Z \tag{4.8}$$

$$PDF[\boldsymbol{\nu}] = \frac{1}{(2\pi)^{n/2}\sqrt{det(\boldsymbol{P}_Z)}} exp\left\{-\frac{1}{2}\boldsymbol{\nu}^T\boldsymbol{P}_Z^{-1}\boldsymbol{\nu}\right\} \tag{4.9}$$

The *computed* measurements instead, can be considered free from noise, since they are artificially generated within the model, and therefore are defined as.

$$\hat{\boldsymbol{z}} = \hat{\boldsymbol{g}}(\hat{\boldsymbol{x}}_0) \tag{4.10}$$

From the definitions of observed and computed measurements vectors, also the formulation for the *residuals* can be obtained as the difference among the two:

$$\delta\hat{\boldsymbol{z}}(\hat{\boldsymbol{x}}_0) = \boldsymbol{z} - \hat{\boldsymbol{z}}(\hat{\boldsymbol{x}}_0) \tag{4.11}$$

Least squares estimation

The batch least square estimation filter is based on the least square method, that aims to find the optimal estimate of the initial state $\hat{\mathbf{x}}_o$ by minimizing a cost function J. Moreover, an *a priori* state vector $\hat{\boldsymbol{x}}_0^0$ must be provided to the filter. Using this vector, allows to improve the efficiency of the estimation preventing it to move toward unrealistic values.

Thus, the cost function is defined as:

$$J(\hat{\boldsymbol{x}}_0) = [\delta\hat{\boldsymbol{z}}(\hat{\boldsymbol{x}}_0)]^T\boldsymbol{W}\delta\hat{\boldsymbol{z}}(\hat{\boldsymbol{x}}_0) + [\hat{\boldsymbol{x}}_0^0 - \hat{\boldsymbol{x}}_0]^T\boldsymbol{W}_0[\hat{\boldsymbol{x}}_0^0 - \hat{\boldsymbol{x}}_0] \tag{4.12}$$

where $\boldsymbol{W}$ and $\boldsymbol{W}_0$ are vectors containing positive semidefinite weights. Their purpose is to assign different importance to:

- residuals and, therefore, measurements in the case of $\boldsymbol{W}$
- *a priori* information in the case of $\boldsymbol{W}_0$

Specifically, larger weights correspond to more relevance being assigned to more reliable measurements, while smaller wights will be assigned to less reliable measurements. Moreover, it is possible to demonstrate that, the weight vectors are defined through the covariance matrices of the residuals and *a priori* information respectively:

$$\boldsymbol{W} = [\boldsymbol{P}_Z]^{-1} \quad , \quad \boldsymbol{W}_0 = [\boldsymbol{P}_0]^{-1} \tag{4.13}$$

and therefore, the least square method is actually a minimum covariance method, where the weights are set by means of the uncertainties on the residuals and *a priori* parameters.

By collecting the measurements and the *a priori* information into a single vector called *modified* measurements vector $\boldsymbol{z}' = \begin{bmatrix} \boldsymbol{z} \\ \hat{\boldsymbol{x}}_0^0 \end{bmatrix}$, it is possible to redefine the cost function in a more compact form:

$$J = (\delta \hat{\boldsymbol{z}}')^T \boldsymbol{W}' (\delta \hat{\boldsymbol{z}}') \tag{4.14}$$

where

$$\boldsymbol{W}' = \begin{bmatrix} \boldsymbol{W} & \mathbf{0}_{m\times n} \\ \mathbf{0}_{n\times m} & \boldsymbol{W}_0 \end{bmatrix} \quad , \quad \delta \hat{\boldsymbol{z}}' = \begin{bmatrix} \boldsymbol{z} - \hat{\boldsymbol{z}} \\ \hat{\boldsymbol{x}}_0^0 - \hat{\boldsymbol{x}}_0 \end{bmatrix} \tag{4.15}$$

The cost function is designed in a way that it uniquely depends on $\hat{\boldsymbol{x}}_0$. Hence a minimum of J can be found using the condition

$$\frac{\partial}{\partial \hat{\boldsymbol{x}}_0} J = \mathbf{0}^T \tag{4.16}$$

Differential correction

Through the latter condition and the definitions of *partials matrix*

$$\boldsymbol{A} = \frac{\partial}{\partial \hat{\boldsymbol{x}}_0} \boldsymbol{z}' \tag{4.17}$$

and the *information matrix*

$$\boldsymbol{H} = \boldsymbol{A}^T \boldsymbol{W} \boldsymbol{A} \tag{4.18}$$

it is possible to build an iterative procedure called *differential correction method*, which, if properly set, converges to an initial state vector that minimizes the cost function and the residuals. Therefore, the differential correction method is an iterative procedure used to refine the estimate of the initial state. The update equation is given by:

$$\hat{\mathbf{x}}_o^{k+1} = \hat{\mathbf{x}}_o^k + \mathbf{H}_k^{-1} \mathbf{A}_k^T \mathbf{W}^T \delta \hat{\mathbf{z}}_k \tag{4.19}$$

where $\delta \boldsymbol{z}_k$ are the residuals computed with the k-th estimation of the initial state vector $\hat{\boldsymbol{x}}_0^k$.

The most common criteria for stopping the differential correction are the following:

$$||\hat{\boldsymbol{x}}_0^{k+1} - \hat{\boldsymbol{x}}_0^k|| < \epsilon_1 \tag{4.20}$$

$$|J^{k+1} - J^k| < \epsilon_2 \tag{4.21}$$

$$||\delta\hat{\boldsymbol{z}}_0^{k+1} - \delta\hat{\boldsymbol{z}}_0^k|| < \epsilon_3 \tag{4.22}$$

Once these criteria are satisfied, the filter has found the optimal configuration of the initial state vector $\hat{\boldsymbol{x}}_0$.

Estimation error and covariance

The optimal initial state vector is not the only output of the estimation filter. Indeed, also the *estimation error covariance matrix* $\boldsymbol{P}(\delta\hat{\boldsymbol{x}}_0)$ is provided at the end of the estimation.

The estimation error $\delta\hat{\mathbf{x}}_o$ is approximated as a Gaussian multivariate random vector and, with this assumption, it is possible to demonstrate that this associated covariance matrix is defined as:

$$\boldsymbol{P}(\delta\hat{\boldsymbol{x}}_0) = [\boldsymbol{A}^T\boldsymbol{W}\boldsymbol{A} + \boldsymbol{W}_0]^{-1} \tag{4.23}$$

where all the matrices are defined by means of the optimal estimation of the initial state vector provided by the differential correction procedure.

In particular, the covariance matrix is made of two contributions:

- information provided by the measurements through $\boldsymbol{A}$ and weighted by $\boldsymbol{W} = [\boldsymbol{P}_Z]^{-1}$
- *a priori* information weighted by $\boldsymbol{W}_0 = [\boldsymbol{P}_0]^{-1}$

It could also be proved that, once additional measurements are introduced, the new covariance matrix is the sum of the single covariance matrices.

4.2 Filter configuration

4.2.1 Mission arc selection

The arc chosen to perform this test goes from the 22^{nd} to the 28^{th} of September 2014 and is part of the Global mapping phase (see Section 1.1.4). In particular, during that week Rosetta initially found itself on a 29 km orbit, carrying out the comet observations to generate the maximum number of *landmarks* and gather data on the environment surrounding 67P. Once the observations were complete and a sufficient amount of *landmarks* were collected, Rosetta could be moved on a closer orbit [29]. Indeed, on the 24^{th}, it performed an OCM, called *GMP-3*, to transfer itself on a 19 km orbit in which the close observation phase started after a few days. Figure 4.1 shows the cometary distance during this part of the mission.

The selection of this arc to perform the estimations comes mainly from two reasons. On one hand, at this point of the mission, Rosetta finished the approach to the comet and was, therefore, gravitationally bound to the comet. Hence, the models can be tested in critical situations, where the S/C dynamics were affected by the cometary environment. On the other hand, the probe was at a distance in which the dynamic environment was still quite stable.

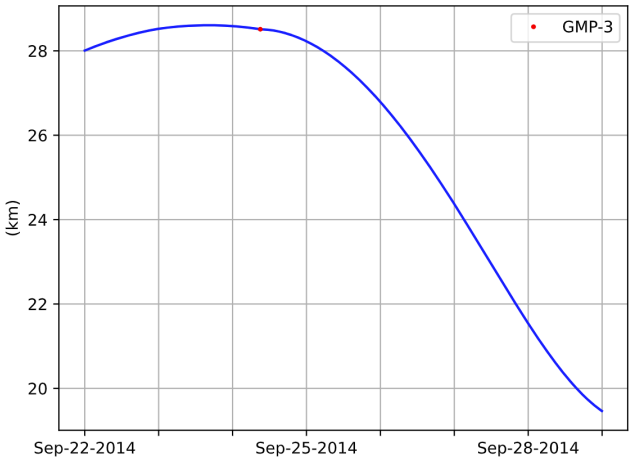

Figure 4.1: Distance of Rosetta from the comet in the Pre-Lander Delivery Phase

4.2.2 Estimated parameters

The type of filter implemented using MONTE is an UD Factorized Covariance Filter [22]. The *solve-for* parameters for which the estimation must be performed are listed in Table 4.1.

Table 4.1: Solve-form parameters of the estimation filter and their *a priori* uncertainties

Parameters	*A priori* σ	Notes
S/C Position	100 km	*A priori* value from *spk* provided by Rosetta's navigation team. It is defined in EME2000.
S/C Velocity	1 m/sec	*A priori* value from *spk* provided by Rosetta's navigation team. It is defined in EME2000.
ΔV of GMP-3	1 - 10 mm/sec	*A priori* value from Godard et al. [14]. σ is approximately 3% of the value.
Right Ascension of GMP-3	2 deg	*A priori* value is set to 0°. It is defined in body frame.
Declination of GMP-3	2 deg	*A priori* value is set to 0°. It is defined in body frame.
Desaturation Manoeuvres	0.333 mm/sec	*A priori* value is zero for all components. They are defined in EME2000 Frame.
Stochastic Accelerations	10^{-10} km/sec^2	*A priori* value is zero for all components. σ is scaled by 0.1 in Y and Z RTN axes. They are defined in EME2000
HGA Phase Center	10 m	*A priori* value is zero meters for each component It is defined in HGA frame

The *a priori* covariances of the *solve for* parameters are chosen to be quite conservative. The *a priori* values and uncertainties for the orbital control and desaturation manoeuvres are selected under the indications of the navigation team [3]. The *a priori* direction of the ΔV provided by GMP-3 is parallel to the S/C Z-axes based on what has been concluded in Section 3.5.2. If such direction is provided in spherical coordinates, it translates into zero right ascension and 0 declination.

4.2.3 Propagator setup

The propagator used to perform the integrations is configured as follows:

- integration tolerance on the velocities in the trajectory equations of 10^{-13}
- minimum integration step of 10^{-6} seconds
- maximum integration step of 8 days
- integration error tolerance scale factor for partials of 10^3

Propagations are carried out using the comet's centre of gravity as the integration centre. The S/C's mass is considered to be constant and equal to 2895.208 kg. This value has been obtained starting from the wet mass of Rosetta provided in its user manual [5] and subtracting the amount of propellant used up to the beginning of the arc. The latter can be extracted within the housekeeping data provided in NASA's small body node [19].

4.2.4 Employed radiometric data

The radiometric data used to perform the estimations are two-way X/X Doppler measurements with 1 second count time. The total number of observables available and the stations from which they are provided are listed in Table 4.2. In this work, only doppler with 60 seconds count time has been used since doppler is the radiometric measurement with more information content on the S/C dynamics with respect to the comet.

As stated in Section 2.1, the measurements are calibrated for the ionosphere and troposphere. Moreover, using the passthrough process, several actions could be carried out on the raw measurements, to prepare them for the estimation. First of all, a manual removal of corrupted data has been performed. Then, an automatic outlier removal process has been applied to the passthrough residuals. The process proceeds as follows

1. Calculate mean μ_i and standard deviation σ_i for the current step
2. Determine the maximum allowed deviation using the formula 4.24. The scale factor N is set to 5 for this analysis. The factor $\pm\delta\sigma$ is used to decide whether residuals are valid or should be discarded to prevent hysteresis. Any residuals outside the range $[\mu_i \pm \Delta\rho_{max}]$ are removed.
3. Repeat until no outliers are present

$$\Delta\rho_{max} = N\left(1 \pm \frac{\delta\sigma}{2}\right)\sigma_i \tag{4.24}$$

Finally, for each tracking pass different weights are assigned to their observables based on their RMS. Tracking passes with higher RMS will be less important than the ones having lower RMS.

Table 4.2: Number of used X/X Doppler measurements from the 22^{nd} to the 28^{th} of September 2014

Provider	Complex	Antenna	# Measurements	Start	End
DSN	Goldstone	DSS 14	1013	03/09/2014	28/10/2014
		DSS 25	187	24/09/2014	24/09/2014
ESTRACK	Malargue	DSA 3	3135	22/09/2014	28/09/2014
	New Norcia	DSA 1	3974	22/09/2014	28/09/2014

Chapter 5

Results

5.1 Estimation without stochastic accelerations

The estimation presented in this section does not account for stochastic accelerations, which, therefore were not either modelled nor estimated. The reason for this choice is the ability of the filter to represent the full system dynamics without using empirical accelerations.

In Figure 5.1 the residuals obtained are shown. It is interesting to notice that no strong signature is present within the residuals, except for two mild ones on September 22 and 23 for the New Norcia station. Indeed, the statistics are promising, with an RMS of 0.062 mm/s which is not far from the results obtained in the passthorugh. Especially because the Doppler measurements used for the estimation have 60-second count time.

The outcome provided by the estimation is shown in Table 5.1. Specifically, it shows the comparison among *a priori* and *a posteriori* parameters (both their values and uncertainties). In particular:

- $R_{X,in}$,$R_{Y,in}$ and $R_{Z,in}$ are the coordinates in EME2000 frame of the initial position of Rosetta with respect to the comet
- $V_{X,in}$,$V_{Y,in}$ and $V_{Z,in}$ are the coordinates in EME2000 frame of the initial velocity of Rosetta with respect to the comet
- X_{pc}, Y_{pc} and Z_{pc} are the coordinates in HGA Frame of the HGA's phase centre
- ΔV_{GMP-3} is the total velocity increment provided GMP-3, while RA_{GMP-3} and DEC_{GMP-3} are the right ascension and declination of the manoeuvre in S/C body frame, giving its direction

From Table 5.1, it can be noticed that the initial state of Rosetta varies by several kilometres among the three coordinates. This confirms the lack of observability using doppler only. Indeed, the residuals fit very well but at the same time, the computed trajectory is quite far from the reference one. The results for the orbital control manoeuvre are also shown in Figure 5.2, from which it can be noted that the estimated manoeuvre is outside the *a priori* uncertainty. In particular, the

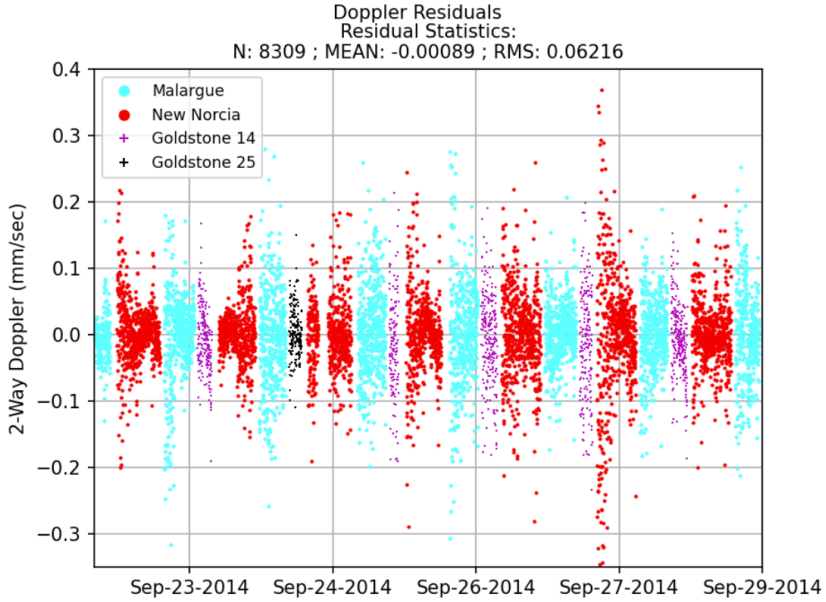

Figure 5.1: X/X Doppler residuals with 60 seconds count time of the period going from September 22 to 28, 2014. To obtain these residuals, no stochastic accelerations have been estimated.

deviation from *a priori* to *a posteriori* ΔV over the *a priori* σ is 2.093. Therefore, the estimated value is still compatible with the one provided by the navigation team.

Table 5.1: *A priori* and *A posteriori* parameters and their uncertainties, obtained through an estimation performed on the arc that goes from September 22 to 28, without evaluating stochastic accelerations

Parameter	*A priori* value	Estimated Value	*A priori* σ	Estimated σ	Units
$R_{X,in}$	2.541×10	2.665×10	1×10^{2}	1.42×10^{-1}	km
$R_{Y,in}$	-1.148	2.354	1×10^{2}	5.453×10^{-1}	km
$R_{Z,in}$	1.082×10	5.951	1×10^{2}	8.810×10^{-1}	km
$V_{X,in}$	3.958×10^{-5}	1.034×10^{-5}	1×10^{-3}	5.067×10^{-6}	km/sec
$V_{Y,in}$	2.99×10^{-5}	2.944×10^{-5}	1×10^{-3}	5.783×10^{-7}	km/sec
$V_{Z,in}$	-1.323×10^{-4}	-1.392×10^{-4}	1×10^{-3}	6.65×10^{-7}	km/sec
ΔV_{GMP-3}	1.6×10^{-5}	1.499×10^{-5}	4.8×10^{-7}	3.7×10^{-7}	km/sec
RA_{GMP-3}	0	-1.272	2	1.668	deg
DEC_{GMP-3}	0	1.548	2	9.483^{-1}	deg
X_{pc}	0	-3.058×10^{-4}	1×10^{-2}	5.766×10^{-5}	km
Y_{pc}	0	-6.975×10^{-5}	1×10^{-2}	1.409×10^{-4}	km
Z_{pc}	0	2.285×10^{-4}	1×10^{-2}	9.837×10^{-3}	km

Regarding the desaturation manoeuvres, their estimated values, together with their uncertainties have been reported in Figure 5.3. The ΔV obtained in this estimation are larger than those calculated by Rosetta's navigation team [3]. The reason could be due to the missing dynamics. Probably, the filter tries to increase the desaturation manoeuvres to absorb the effects of the coma drag.

As a last remark, the state covariance evolution is shown in Figure 5.4. The

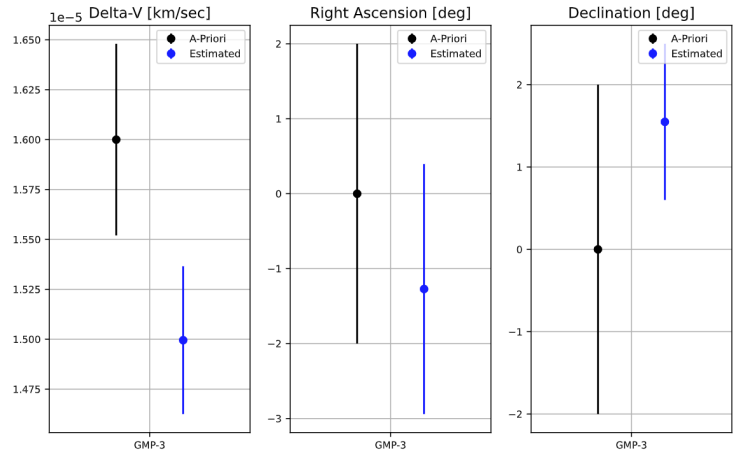

Figure 5.2: *A priori* and *a posteriori* parameters of the GMP-3 manoeuvre for the estimation without stochastic accelerations

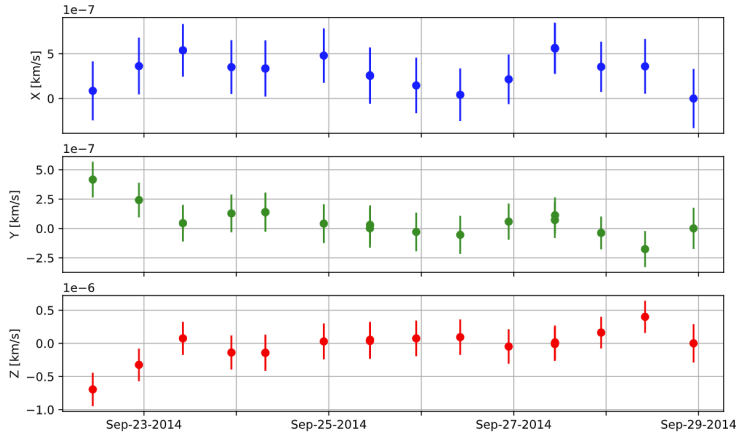

Figure 5.3: Desaturation manoeuvres' velocity increments in EME2000 Frame obtained in the estimation without stochastic accelerations

uncertainties on position go from a few meters to several hundred meters, while the ones obtained by the navigation are 10-30 meters. The uncertainties on velocity, instead, are of a few mm/sec as the ones of the navigation team. Therefore, it is clear how using doppler observables only lacks information in terms of instantaneous position, which, in the case of Rosetta's navigation team, is retrieved also using the optical navigation subsystem.

5.2 Estimation with constant stochastic accelerations

In the second case analysed, stochastic accelerations have been implemented and estimated. In particular, they are modelled as 2 hours batches with constant value within the individual batch.

From the residuals in Figure 5.5, a slight improvement can be observed. Indeed, both mean and RMS are smaller. Similarly, the signatures that could be noticed in

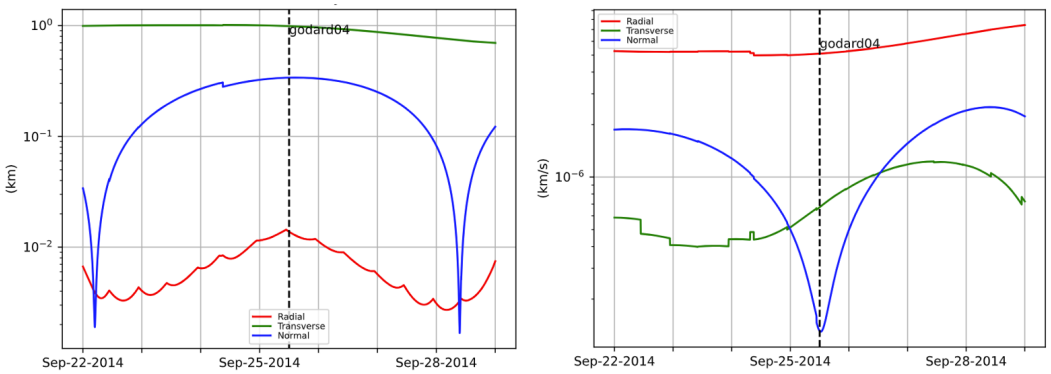

Figure 5.4: State covariance estimation without stochastic accelerations in RTN frame. Left: position; right: velocity.

the previous set of residuals, are almost not visible any more. This means that the stochastic accelerations have been able to absorb those dynamic events responsible for such signatures.

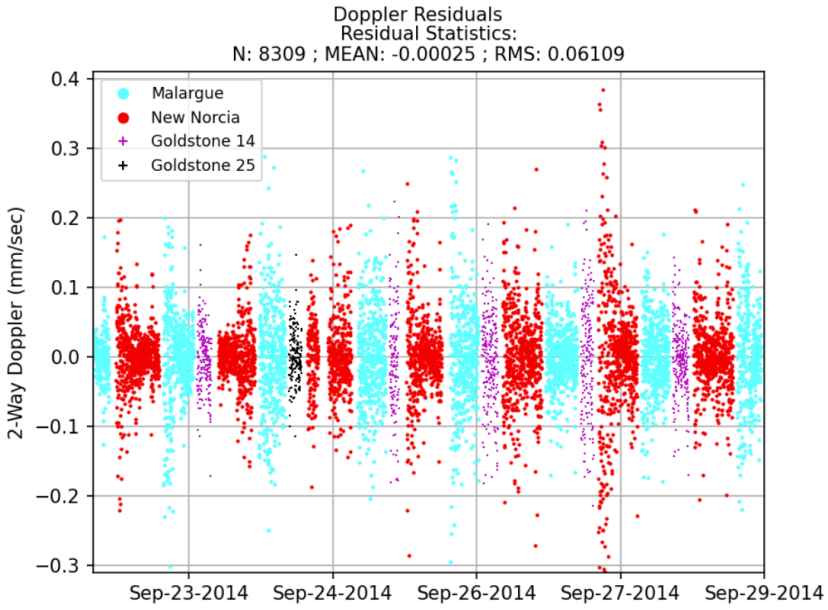

Figure 5.5: X/X Doppler residuals with a 60-second count time of the period going from September 22 to 28, 2014. In this case, 2-hour batches of stochastic accelerations with constant values have been implemented and estimated.

Concerning the estimation of the parameters, from Table 5.2 it can be seen that the performance and results of the filter have indeed been affected. Rosetta's initial position has moved a few kilometres and also its initial velocity is slightly different. The *a posteriori* value of the phase centre, instead is very similar. Finally, it is interesting to notice, using Figure 5.6, that the ΔV provided by the OCM is larger than the one obtained without the stochastic accelerations and is now within the *a priori* uncertainty (1-σ).

Table 5.2: *A priori* and *A posteriori* parameters and their sigmas, obtained through an estimation performed on the arc that goes from September 22 to 28, using stochastic accelerations.

Parameter	*A priori* value	Estimated Value	*A priori* σ	Estimated σ	Units
$R_{X,in}$	2.541×10	2.639×10	1×10^{2}	3.046×10^{-1}	km
$R_{Y,in}$	-1.148	3.621	1×10^{2}	8.473×10^{-1}	km
$R_{Z,in}$	1.082	3.697	1×10^{2}	1.430	km
$V_{X,in}$	3.958×10^{-5}	-1.722×10^{-5}	1×10^{-3}	8.063×10^{-6}	km/sec
$V_{Y,in}$	2.990×10^{-5}	2.653×10^{-5}	1×10^{-3}	1.497×10^{-6}	km/sec
$V_{Z,in}$	-1.323×10^{-4}	-1.378×10^{-4}	1×10^{-3}	1.071×10^{-6}	km/sec
ΔV_{GMP-3}	1.6×10^{-5}	1.539×10^{-5}	4.8×10^{-7}	4.172×10^{-7}	km/sec
RA_{GMP-3}	0	7.285×10^{-1}	2	1.898	deg
DEC_{GMP-3}	0	1.827	2	1.040^{-1}	deg
X_{pc}	0	-3.061×10^{-4}	1×10^{-2}	5.766×10^{-5}	km
Y_{pc}	0	-7.238×10^{-5}	1×10^{-2}	1.409×10^{-4}	km
Z_{pc}	0	2.429×10^{-4}	1×10^{-2}	9.837×10^{-3}	km

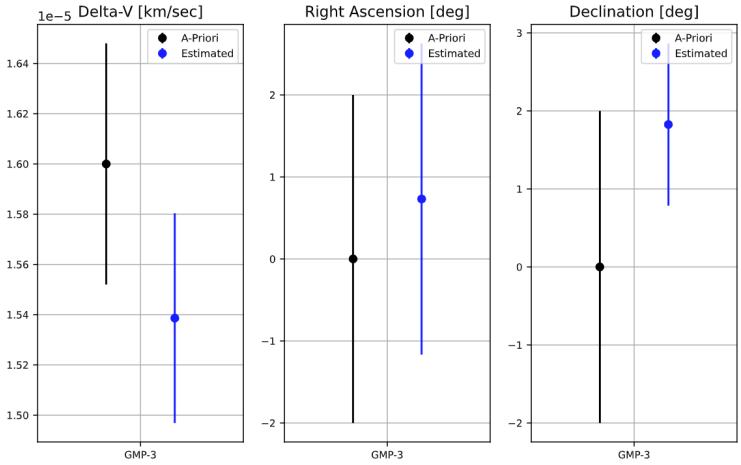

Figure 5.6: *A priori* and *a posteriori* parameters of the GMP-3 manoeuvre for the estimation with stochastic accelerations

The same can be said for desaturation manoeuvres, whose ΔV has become even smaller than the ones of the navigation team. Stochastic accelerations either provide a more reasonable estimation or absorb a portion of the manoeuvres' speed increment. Anyway, the new values are much closer to the navigation team's ones, as shown in Figure 5.7.

Then, the values of the estimated stochastic accelerations and their *a posteriori* sigma are shown in Figure 5.8. As expected, the greatest accelerations act in the radial direction, i.e. in the direction in which the gas composing the coma is ejected by the comet. The magnitude of the estimated acceleration is larger than the one expected by the coma drag model used by the navigation team (see Figure 3.1). The other components are weaker than the radial one by one order of magnitude, which is coherent with the expected behaviour.

Finally, from Figure 5.9, the evolution of the state covariance can be observed. Introducing the stochastic accelerations, the number of degrees of freedom of the

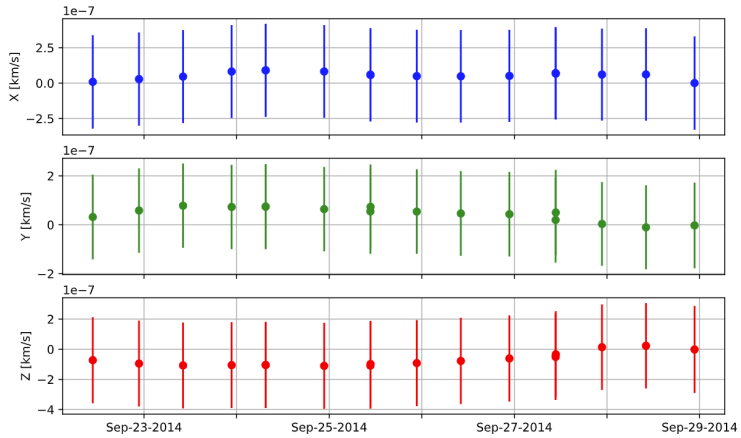

Figure 5.7: Desaturation manoeuvres' velocity increments in EME2000 Frame obtained in the estimation with stochastic accelerations

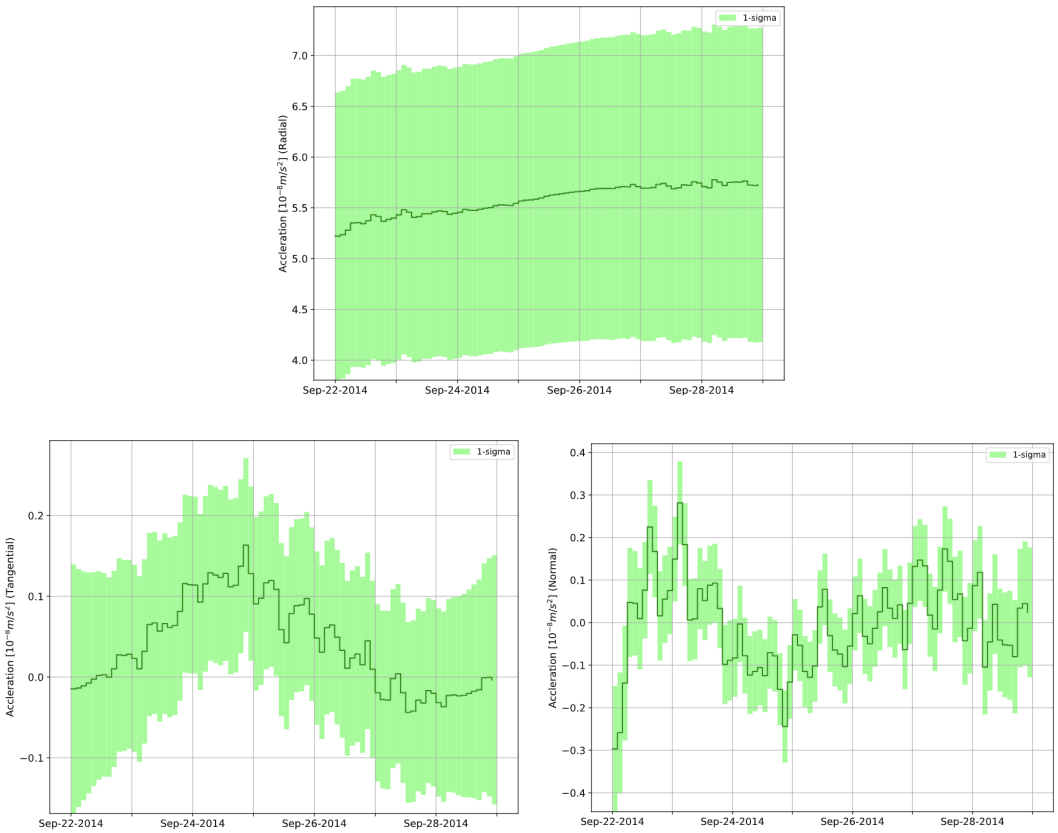

Figure 5.8: Estimated piecewise constant stochastic accelerations and their uncertainty (1-σ)

system considerably increased, which leads to a general worsening of the uncertainties on the S/C state.

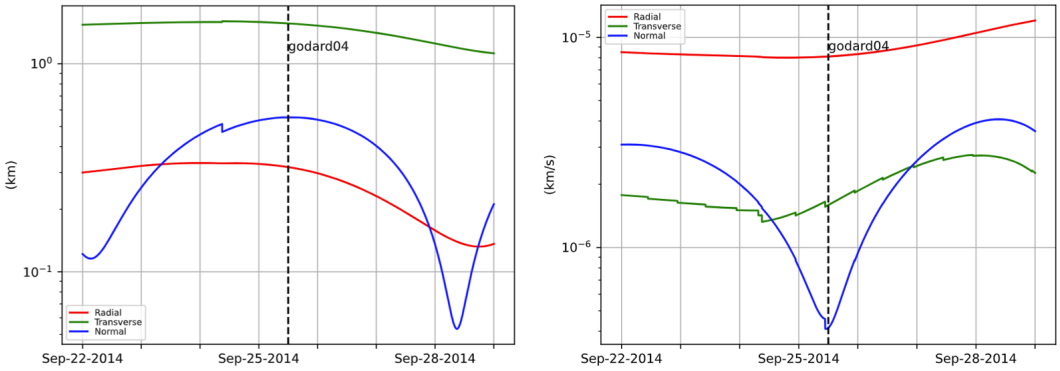

Figure 5.9: State covariance estimation with stochastic accelerations in RTN Frame. Left: position; right: velocity.

Chapter 6

Conclusions and future work

The study presented in this work aimed at creating a simulation environment for a deep analysis of the radiometric measurements collected by the Rosetta mission. In particular, the goal was to investigate the dynamics that the probe experienced while escorting comet 67P Churyumov-Gerasimenko on its journey close to the Sun, allowing us to learn more about the comet itself and its outgassing activity.

At first, a passthrough process has been pursued. Such a procedure consists of taking the reference trajectory provided by the navigation team of the mission, using it to simulate the generation of radiometric measurements and comparing them with the real ones. By comparing the computed and real measurements, it is possible to highlight the imperfections of the observational model and, therefore, improve its performance. Indeed, using the passtrough it has been possible to increase the reliability of radiometric measurements significantly. For instance, modelling the HGA movements has proven to be crucial, particularly concerning the precision of Doppler measurements. Moreover, the estimation of the ground station biases confirmed the reliability of the observational model, since they matched the value obtained by the navigation team of Rosetta.

Afterwards, the dynamical model has been computed. The gravity of 67P was generated using spherical harmonics up to degree three and also the gravitational contributions of the Sun (up to degree two), planets, Earth, Moon and Pluto have been accounted for, together with their relativistic corrections. To model the solar radiation pressure, it has been necessary to define the spacecraft surfaces with their optical coefficients. Both orbital and desaturation manoeuvres were included in the dynamics. The last important force acting on the probe is the coma drag, i.e. the acceleration generated by the interaction between the spacecraft surfaces and the gas ejected from the comet. Its contribution has been introduced in the model using stochastic accelerations of two-hour batches in which they assume constant values.

Finally, the simulation environment was ready to be tested on a mission arc of one week in which Rosetta is gravitationally bound to the comet, but still not too close to 67P, where dynamics become particularly complex. Therefore, estimations have been performed on the spacecraft state, the orbital and desaturation manoeuvres, the high gain antenna's phase centre location and the stochastic accelerations modelling the coma drag.

These estimations proved that the model is trustworthy, but, at the same time, they highlighted its limits. In particular, using only radiometric measurements

precludes the possibility of observing the dynamics of the spacecraft while staying very close to the comet. Nevertheless, the addition of stochastic accelerations has improved the general behaviour of the model, getting closer to the real picture.

Although the implemented dynamical model fits the data well, future analyses should focus on improving its fidelity. The most important tasks that should be carried out in this regard are the following:

- Implement a *coma drag model* of Rosetta. A good start would be to reproduce the same model of Rosetta's navigation team, which models the drag as a radial acceleration. It depends on the coma density which, as a first approximation, follows an inverse square law with the cometocentric distance. In addition, the acceleration linearly depends on the S/C cross-sectional area facing the comet. Such a model was used by the navigation team in the orbit determination phase. Afterwards, they could use ROSINA measurements to withdraw the coma's density and with such data, they could improve the accuracies of their first iteration. Hence, using ROSINA data, which can be downloaded by anyone, is another very interesting task that could be carried out.

- Use *optical navigation data*. Indeed, Rosetta was equipped with a very advanced optical navigation system consisting of 4 cameras. As mentioned in Section1.1.4, this subsystem aimed to obtain some recognizable surface features of 67P called *landmarks*, and use them to get the comet to S/C position, aiding the orbit determination process. During this work, low observability has been one of the main limits and enhancing the orbit determination with the optical measurements seems to be crucial, especially in all those cases where the dynamic environment becomes particularly complex.

- Concerning the observational model, it would be useful to estimate the *Marini Effect*, i.e. the deviation of real observables (particularly Doppler) due to the body rotation of the S/C. Taking it into account would improve radiometric measurements' precision even more. In this regard, also using IFMS's meteorological data to calibrate Doppler and Range measurements for the Troposphere would benefit the data's reliability.

Bibliography

[1] K.-H. Glassmeier, H. Boehnhardt, D. Koschny, E. Kührt, and I. Richter, "The rosetta mission: flying towards the origin of the solar system," *Space Science Reviews*, vol. 128, pp. 1–21, 2007.

[2] C. L. Thornton and J. S. Border, *Radiometric tracking techniques for deep-space navigation*. John Wiley & Sons, 2003.

[3] B. Godard, F. Budnik, P. Munoz, T. Morley, and V. Janarthanan, "Orbit determination of rosetta around comet 67p/churyumov-gerasimenko," in *Proceedings 25th International Symposium on Space Flight Dynamics–25th ISSFD, Munich, Germany*, 2015.

[4] R. Team, *Rosetta Users Manual*, 2003.

[5] M. Richner, G. Gebauer, and T. Leissle, *Coordinates Systems For Rosetta*, 2003.

[6] T. Kato and J. C. van der Ha, "Precise modelling of solar and thermal accelerations on rosetta," *Acta Astronautica*, vol. 72, pp. 165–177, 2012.

[7] L. O'Rourke, *Science User Guide for the ROSETTA HK Engineering data*, 2019.

[8] T. Morley and F. Budnik, "Rosetta navigation at its first earth swing-by," in *Proceedings of the International Symposium on Space Technology and Science*, vol. 25. Citeseer, 2006, p. 593.

[9] F. Budnik and T. Morley, "Rosetta navigation at its mars swing-by," in *Proceedings of the 20th International Symposium on Space Flight Dynamics*, 2007.

[10] T. Morley and F. Budnik, "Rosetta navigation for the fly-by of asteroid 2867 šteins," in *Proceedings 21st International Symposium on Space Flight Dynamics-21st ISSFD, Toulouse, France*, 2009.

[11] T. Morley, F. Budnik, M. Croon, and B. Godard, "Rosetta navigation for the fly-by of asteroid 21 lutetia," in *Proceedings 23rd International Symposium on Space Flight Dynamics-23rd ISSFD, Pasadena, USA*, 2012.

[12] T. Morley, F. Budnik, B. Godard, P. Muñoz, and V. Janarthanan, "Rosetta navigation from reactivation until arrival at comet 67p/churyumov-gerasimenko," in *Proceedings 25th International Symposium on Space Flight Dynamics–25th ISSFD, Munich, Germany*, 2015.

[13] P. Muñoz, F. Budnik, V. Companys, B. Godard, C. M. Casas, T. Morley, and V. Janarthanan, "Rosetta navigation during lander delivery phase and reconstruction of philae descent trajectory and rebound," in *25th International Symposium on Space Flight Dynamics*, 2015, pp. 1–20.

[14] B. Godard, F. Budnik, G. Bellei, P. Muñoz, and T. Morley, "Multi-arc orbit determination to determine rosetta trajectory and 67p physical parameters," in *Proceedings 26th International Symposium on Space Flight Dynamics–26th ISSFD, Matsuyama, Japan*, 2017.

[15] P. Muñoz, V. Companys, F. Budnik, B. Godard, D. Pellegrinetti, G. Bellei, R. Bauske, and W. Martens, "Rosetta navigation during the end of mission phase," in *2017 International Symposium on Space Flight Dynamics, Matsuyama, Japan, ISSFD-2017-015*, 2017.

[16] S. Tellmann, *Rosetta Radioscience Investigations (RSI) - Experiment User Manual*, 2006.

[17] B. Semenov, F. Tosi, J. L. Vazquez, B. Grieger, B. Maud, M. Costa Sitija, A. Escalante, and R. Valles, "Rosetta spacecraft and rosetta lander frames kernel." [Online]. Available: https://naif.jpl.nasa.gov/pub/naif/ROSETTA/kernels/fk/ROS_V38.TF

[18] "Monte." [Online]. Available: https://montepy.jpl.nasa.gov/

[19] "Nasa pds: Small bodies node." [Online]. Available: https://pds-smallbodies.astro.umd.edu/

[20] M. Ricart, *IF and Modem System - Interface Control Document*, 2006.

[21] *Tracking Data Message - Recommended Standard*, 2020.

[22] *MONTE Documentation.*

[23] M. Zannoni, "Deep space navigation lecture notes," 2023.

[24] T. Runge, *Media Calibration Interface*, 2008.

[25] "Naif." [Online]. Available: https://naif.jpl.nasa.gov/naif/index.html

[26] "Rosetta orbiter - instrument host information." [Online]. Available: https://naif.jpl.nasa.gov/pub/naif/pds/data/ro_rl-e_m_a_c-spice-6-v1.0/rossp_1000/CATALOG/INSTHOST.CAT

[27] N. Fougere, K. Altwegg, J.-J. Berthelier, A. Bieler, D. Bockelee-Morvan, U. Calmonte, F. Capaccioni, M. R. Combi, J. De Keyser, V. Debout *et al.*, "Three-dimensional direct simulation monte-carlo modeling of the coma of comet 67p/churyumov-gerasimenko observed by the virtis and rosina instruments on board rosetta," *Astronomy & Astrophysics*, vol. 588, p. A134, 2016.

[28] C. Bielsa, M. Müller, and U. Herfort, "Operational approach for the modeling of the coma drag force on rosetta," in *24th International Symposium on Space Flight Dynamics*, 2014.

[29] A. Accomazzo, P. Ferri, S. Lodiot, J.-L. Pellon-Bailon, A. Hubault, R. Porta, J. Urbanek, R. Kay, M. Eiblmaier, and T. Francisco, "Rosetta operations at the comet," *Acta Astronautica*, vol. 115, pp. 434–441, 2015.